J. Biosci. Public Health 2026; 2(1):96-123

JBPH

Open access

Journal of Biosciences and Public Health

eISSN: 3104-8749

DOI: https://doi.org/10.5455/JBPH.2026.03

Published by: www.4greenresearch.org

Original Research

Unlocking Genomics of Multifunctional Endophytic Strain *Citrobacter* sp. HSTU-ABk15 from Rice Focusing Pesticide Bioremediation and Plant Health

Bissas Binduraz[1±], Sukumar Roy[1±], Md. Abullah-Al-Mamun[2], Md. Shohorab Hossain[3], Aminur Rahman[4], Md. Amirul Islam Abir[1], Mst. Tahsin Sultana[1], Sibdas Ghosh[5], Md. Golam Mortuza[6], Kye Man Cho[7], Md. Azizul Haque[1]*

[±]**Both authors have equal contribution to the work**

[1]Department of Biochemistry and Molecular Biology, Hajee Mohammad Danesh Science and Technology University, Dinajpur 5200, Bangladesh
[2]Yunnan Institute of Parasitic Diseases (YIPD), Chenggong District, Kunming Municipality, Yunnan, 650500, P.R. China
[3]Department of Biochemistry and Molecular Biology, Trust University, Barishal, Bangladesh
[4]Department of Biomedical Sciences, College of Clinical Pharmacy, King Faisal University, Al-Ahsa 31982, Saudi Arabia
[5]Albany College of Pharmacy and Health Sciences, 106 New Scotland Avenue, Albany, NY 12208, United States of America
[6]Department of Biochemistry and Molecular Biology, Faculty of Agriculture, Bangladesh Agricultural University, Mymensing, Bangladesh
[7]Department of GreenBio Science and Agri-Food Bio Convergence Institute, Gyeongsang 11 National University, Jinju 52727, Republic of Korea

Article information
Received: December 08, 2025
Revised: December 30, 2025
Accepted: December 31, 2025
Published: January 04, 2026

***Corresponding author**
Department of Biochemistry and Molecular Biology, Hajee Mohammad Danesh Science and Technology University, Dinajpur5200, Bangladesh
E-mail: helalbmb2016@hstu.ac.bd
ORCID ID: https://orcid.org/0000- 0002-9788-0766

Keywords: Endophytic bacteria, plant growth promotion, *Citrobacter* sp., In-silico bioremediation, organophosphate-degrading genes, genomic analysis

Cite this article: Binduraz B, Roy S, Abullah-Al-Mamun M, Hossain MS, Rahman A, Abir MAI, Sultana MT, Ghosh S, Mortuza MG, Cho KM, Haque MA. Unlocking genomics of multifunctional endophytic strain *Citrobacter* sp. HSTU-ABk15 from rice focusing pesticide bioremediation and plant health. *J Biosci Public Health*. 2026;2(1):96-123. doi:10.5455/JBPH.2026.03

ABSTRACT

Endophytic bacteria represent a promising biological solution for sustainable agriculture and pesticide bioremediation. This study reports the isolation and comprehensive characterization of the novel endophytic bacterial strain *Citrobacter* sp. HSTU-ABk15 from *Oryza sativa* L. tissues exposed to pesticide stress. Integrated biochemical, genomic, and *in silico* analyses revealed their dual functionality in chlorpyrifos degradation and plant growth promotion. The genome sequence analysis (ANI, dDDH, pangenomics, Progressive Mauve, and phylogenetic analysis) confirmed the strains belong to the *Citrobacter* species. The isolates exhibited phosphate solubilization, indole-3-acetic acid (IAA) production, and 1-aminocyclopropane-1-carboxylate (ACC) deaminase-producing genes in their annotated genome. Genome annotation identified organophosphate-degrading genes (*opd*, *phn*, *ampD*, *pepD*), suggesting potential for pesticide degradation. *In silico* docking analyses validated strong interactions (–6.5 to –8.0 kcal·mol^{-1}) between key enzymes (AmpD, PepE, GlpQ, carboxylesterase, amidohydrolase, and phosphonatase) and cypermethrin, diazinon, and crotoxiphos. Phylogenomic analyses (ANI and dDDH) confirmed their distinct taxonomic positions, indicating functionally distinct endophytic strains. *Citrobacter* sp. strain HSTU-ABk15 as a genetically robust, multifunctional endophyte with significant potential for eco-friendly pesticide remediation and sustainable rice cultivation.

1. INTRODUCTION

Feeding a global population that is expected to reach 10 billion by 2050 challenges modern agriculture. Meeting this demand requires adopting sustainable farming practices to ensure food security, conserve resources, and reduce environmental harm [1, 2]. Developing and using innovative, environmentally responsible alternatives to chemical pesticides, such as new antimicrobial bioactive compounds, is essential. Overusing chemical pesticides causes new pest outbreaks, harms non-target species, and leaves persistent residues in soil and water [3]. The demand for better antimicrobial agents underscores the importance of such alternatives. These challenges make agricultural innovation focused on sustainability and environmental responsibility urgent. Beneficial microorganisms, particularly bacterial endophytes, are essential for sustainable crop production. These bacteria inhabit plant tissues without causing harm and form symbiotic relationships that enhance plant growth and stress tolerance [4]. They promote growth by fixing nitrogen, increasing phosphate availability, and producing plant hormones such as auxins, gibberellins, and cytokinins [4]. Nitrogen-fixing endophytes, including *Novosphingobium sediminicola*, *Ochrobactrum intermedium*, *Bradyrhizobium*, *Kosakonia*, and *Paraburkholderia, contribute to* nutrient cycling and improve soil fertility [4]. Endophytes also help plants resist stress by producing lytic enzymes, siderophores, and antioxidants, or by activating plant defenses against disease [5]. Additionally, endophytic bacteria support environmental remediation by degrading organic pollutants, including pesticides, dyes, and other xenobiotics. They achieve this by adsorbing pollutants, internalizing them, and using enzymes to convert them into less harmful substances [6]. Bacteria from genera such as *Bacillus*, *Acinetobacter*, *Enterobacter*, *Serratia*, *Pseudomonas*, *Flavobacterium*, and *Sphingomonas can degrade th*e pesticide chlorpyrifos [7, 8].

Endophytic bacteria are an important source of bioactive secondary metabolites, such as alkaloids, phenols, flavonoids, peptides, steroids, and terpenoids. Many of these compounds have antimicrobial, antifungal, antitumor, and anticancer effects [4,9]. Recent advances in genome mining and bioinformatics tools, such as antiSMASH, have enabled the identification of a wide range of biosynthetic gene clusters (BGCs) associated with these metabolites [10]. These genomic studies also help find genes that support plant growth, nutrient uptake, and stress tolerance [4]. Although endophytes are known for their many functions, there remains a significant research gap in fully characterizing new strains of important crops such as rice (*Oryza sativa* L.). Most research has focused on single aspects, such as plant growth promotion, pollutant breakdown, or secondary metabolite production.

However, only a few studies have used a genome-based approach to explore the combined abilities of new endophytes. The present study addresses this gap by isolating and characterizing a novel bacterial endophyte, *Citrobacter* sp. HSTU-ABk15, from rice tissues. The study aimed to (i) identify and classify the isolates through metabolic profiling and whole-genome sequencing; (ii) evaluate their plant growth-promoting traits, including nitrogen fixation, phosphate solubilization, and phytohormone-producing genes; (iii) assess their chlorpyrifos degradation potential using *in silico* protein modelling and molecular docking. These findings provide new insights into the multifunctional potential of rice-associated endophytic bacteria and highlight their applications in sustainable agriculture, bioremediation, and the discovery of novel bioactive compounds.

2. MATERIALS AND METHODS

2.1. Isolation and biochemical characterization

Endophytic bacteria, *Citrobacter* sp. HSTU-ABk15, was isolated from surface-sterilized roots of healthy rice (*Oryza sativa* L.) following established protocols [11, 12]. Specifically, isolation was performed on chlorpyrifos-enriched minimal salt agar containing 0.2% chlorpyrifos to select for pesticide-tolerant endophytes. Subsequently, purified colonies were characterized biochemically according to *Bergey's Manual* (1996) using catalase, oxidase, citrate utilization, urease, and triple sugar iron tests [13]. Finally, hydrolytic enzyme activities (cellulase, xylanase, pectinase) were assessed by clear-zone formation on specific agar plates [14].

2.2. Genomic analysis of *Citrobacter* sp. HSTU-ABk15: DNA extraction, whole genome sequencing, assembly, and annotation

Genomic DNA of the strain was isolated using the Promega (USA) Genomic DNA Extraction Kit following the manufacturer's protocol. DNA purity and concentration were assessed with a Promega DNA spectrophotometer. Whole-genome shotgun sequencing of the *Citrobacter* sp. isolate was carried out on the Illumina MiniSeq platform (Illumina, USA) using paired-end sequencing chemistry. Genomic libraries were prepared from purified DNA using the Nextera XT Library Preparation Kit according to standard procedures.

Raw reads were quality-checked with FASTQC v1.0.0, and adapter removal, quality trimming, and length filtering were performed using the FASTQ Toolkit. After filtering, approximately 248.95 Mbp of high-quality data were assembled de novo using SPAdes v3.9.0 to generate contigs, which were subsequently arranged into scaffolds. The assembled sequences were further refined and aligned using Progressive Mauve v2.4.0. Genome annotation was performed using both the NCBI Prokaryotic Genome Annotation Pipeline (PGAP v4.5) and Prokka. Multilocus sequence typing (MLST and pMLST) was conducted through the Illumina Bacterial Analysis Pipeline v1.0.4. Functional categorization of predicted protein-coding genes was performed using the COG database via the RAST annotation server. Functional insights were derived from PGAP annotations [14, 15]. Phylogenetic relationships based on housekeeping genes (recA, gyrB, and rpoB) were inferred using MEGA XI with 1,000 bootstrap replications. Genes involved in nitrogen fixation, phosphate solubilization, phytohormone biosynthesis, biofilm formation, and abiotic stress tolerance were identified by the following approaches [15].

2.2. Virtual screening and catalytic triad visualization

We retrieved the three-dimensional structures of the organophosphate insecticides used in this study from the PubChem database (https://pubchem.ncbi.nlm.nih.gov/) and compiled them before virtual screening. We optimized the ligand structures and minimized their energy using the MMFF94 force field with the steepest-descent algorithm. Virtual screening was performed in PyRx, in which each ligand was docked to the selected protein targets. For each enzyme, we ran multiple docking simulations to find possible active-site interactions and confirm binding patterns. We exported the binding affinities (kcal/mol) and visualized them in R. Enzymes with docking scores above 7 kcal/mol were studied further, and we created close-up images of the catalytic centers, such as Ser-His-Asp and Ser-His-His triads, to explore possible mechanisms of insecticide degradation.

2.3. Protein modeling and docking

Candidate pesticide-degrading enzymes were, identified and three-dimensional structures were, predicted using the SWISS-MODEL and I-TASSER platforms [16]. The quality and structural reliability of the modeled proteins were evaluated through multiple validation tools, including ERRAT, VERIFY-3D, and Ramachandran plot analysis. Molecular docking analyses were performed using PyRx and Discovery Studio to investigate enzyme–ligand interactions. The docking results demonstrated strong binding affinities, with calculated binding energies ranging from −6.5 to −8.0 kcal·mol^{-1}, and identified key catalytic residues potentially involved in chlorpyrifos degradation [17, 18].

2.4. Comparative genomic analyses: Phylogenetic analyses and average nucleotide identity (ANI)

Housekeeping genes (16S rRNA, rpoB, recA, and gyrB, which are essential for basic cellular function) were extracted from the draft genome, aligned individually, and concatenated for phylogenetic reconstruction. Neighbor-joining trees (phylogenetic trees built using a distance-based method) for both the 16S rRNA gene and the concatenated markers were generated in MEGA X (a molecular evolutionary genetics analysis software). Whole-genome phylogeny (evolutionary relationship analysis using the entire genome) was constructed using REALPHY 1.12 (http://www.realphy.unibas.ch/realphy/), incorporating the genome of the strain and those of its nearest relatives. ANI values (Average Nucleotide Identity, a measure of genomic similarity; specifically, ANIb refers to BLAST-based ANI) between Citrobacter sp. HSTU-ABk15 and closely related taxa were calculated using the JSpeciesWS platform (http://jspecies.ribhost.com/jspeciesws).

2.5. Digital DNA–DNA hybridization (dDDH)

Genome similarity was further assessed by digital DNA–DNA hybridization using the Genome-to-Genome Distance Calculator (GGDC 3.0; https://ggdc.dsmz.de/), comparing the target strain with 14 phylogenetically related *Citrobacter* genomes [14, 15].

2.6. Genome alignment (MAUVE)

Whole-genome alignment across Citrobacter genomes was executed using the MAUVE algorithm to visualize syntenic regions and structural variations. Colored synteny blocks facilitated comparison of genome architecture. Pangenome analysis was additionally performed using publicly available servers as described by [12] to evaluate gene distribution patterns across species [14, 15].

2.7. Genome-level comparison

To explore genomic features, the draft genome of Citrobacter sp. HSTU-ABk15 was compared to closely related, recently reported Citrobacter genomes. Circular and linear genome visualizations were generated using CGView (http://www.cgview) and BRIG v0.95, respectively. BLAST+ analyses (70–90% identity threshold; E-value 10) were run to map sequence similarity. Genome collinearity and synteny were assessed using Progressive Mauve (http://darlinglab.org/mauve/mauve.html). In silico DNA–DNA hybridization with the 15 closest genomes was performed using the GGDC server [14, 15].

2.8. Functional Genes: Plant growth promotion, stress tolerance, and insecticide degradation

Plant growth-promoting traits encoded in *Citrobacter* genomes were mined from PGAP-annotated files and compared with those of reference endophytic strains. Genes associated with nitrogen fixation (e.g., nifA–nifZ, iscAUR), nitrosative stress tolerance (norRV, ntrB, glnK, nsrR), ammonia assimilation, ACC deaminase production, siderophore biosynthesis (enterobactin), indole-3-acetic acid (IAA) synthesis, phosphate metabolism, sulfur assimilation, biofilm formation, chemotaxis, root colonization, trehalose metabolism, antioxidant defense (e.g., superoxide dismutase), hydrolase activity, adhesin formation, symbiosis-related pathways, and antimicrobial peptide synthesis were identified. Genes linked to abiotic stress tolerance such as cold-shock, heat-shock, drought-stress, and heavy-metal resistance determinants were also catalogued. Furthermore, organophosphate-degrading genes, including carboxylesterase, organophosphorus hydrolase (*opd*), amidase, phosphonatase, phosphotriesterase, and phosphodiesterase, were identified from the literature and curated accordingly [19, 20].

3. RESULTS

3.1. Biochemical characterization of the newly isolated endophytic bacteria

Three bacterial strains; *Citrobacter* sp. HSTU-ABk15, isolated from rice plants were biochemically characterized (**Table 1**). All strains were positive for oxidase, citrate utilization, catalase, urease, TSI, and carbohydrate (lactose, sucrose, dextrose) utilization, but negative for indole. Motility and indole/urease test results varied among strains. In the Methyl red test, HSTU-ABk15 was negative, while the opposite pattern was observed in the Voges-Proskauer test. The strain displayed xylanase, amylase, CMCase and protease activity.

Table 1. Biochemical test of *Citrobacter* sp. HSTU-ABk15.

	Oxidase	Citrate	Catalase	MIU	Mortality	Urease	VP	MR	TSI	Lactose	Sucrose	Dextrose	Maltose	CMCase	Xylanase	Amylase	Protease
Citrobacter sp. HSTU-ABk15	+	+	+	-	-	-	+	-	+	+	+	+	+	+	+	+	+

3.2. Genome sequencing of the strain

Fast QC quality assessment of the paired-end raw reads (R1 and R2) generated from Illumina sequencing showed a GC content of 53.4%, which falls within the acceptable range (40–70%) for high-quality bacterial genomes (**Table 2**). The filtered reads were assembled de novo using SPAdes v3.9.0, producing 573 contigs with a total genome size of approximately 4.75 Mb.

Table 2. Genomic feature of the strain *Citrobacter* sp. HSTU-ABk15.

Features	Annotation statistics
Genome	*Citrobacter* sp. HSTU-ABk15
Domain	Bacteria
Taxonomy	Bacteria; *Citrobacter* sp. HSTU-ABk15
Size	4,754,666
GC content	53.4
N50	198784
L50	8
Number of contigs (with PEGs)	131
Number of subsystems	573
Number of coding's sequences	4375
Number of RNAs	100

The draft genome of *Citrobacter* sp. HSTU-ABk15 comprised a single circular chromosome without plasmids (**Figure 1A**). Annotation through PGAP identified 4,375 protein-coding genes and 100 RNA genes. RAST analysis further revealed key assembly statistics, including an N50 of 198,784 bp and an L50 of 8. Subsystem distribution indicated that approximately 63% of the genome was assigned to functional categories, while the remaining 37% consisted of genes outside defined subsystems (**Figure 1B)**. Major functional groups included genes involved in amino acid metabolism (451), carbohydrate metabolism (725), and protein metabolism (302), highlighting the metabolic versatility of the strain.

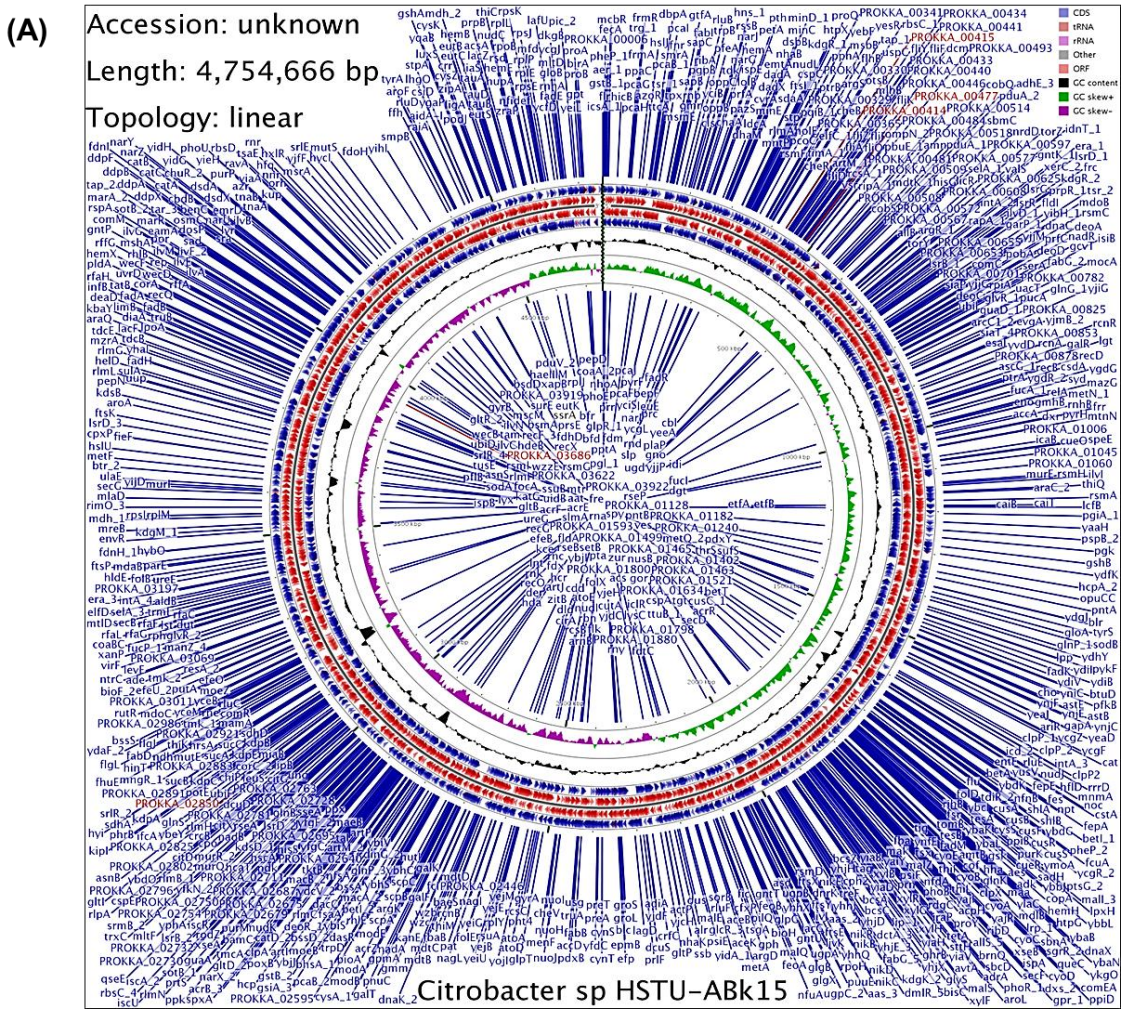

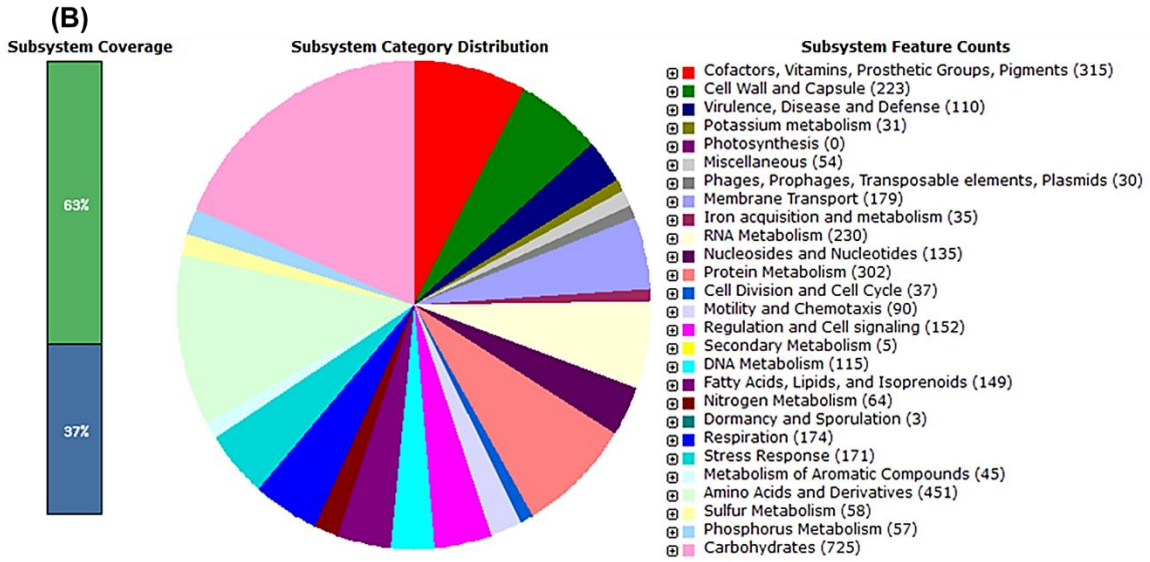

Figure 1. Genome annotation map of *Citrobacter* sp. HSTU-ABk15. A) Circular genome map of *Citrobacter* sp. HSTU-ABK15 showing gene distribution on forward and reverse strands, RNA features, GC content, and GC skew for the 4.75 Mb linear chromosome constructed using Linux programming. B) Subsystem coverage and functional category distribution of the genome annotated using the RAST (SEED) server.

3.3. Average nucleotide identity (ANI) of the strain

Average nucleotide identity (ANI) is study to the most relevant comparative parameter used for bacterial species determination. *Citrobacter* sp. HSTU-ABk15 genome was compared with 14 different closely related bacterial species where maximum result shown up 98% nucleotide sequence identity with CP 014070.2, CP057150.1, CP057632.1, CP064180.1, LORU02000001.1, CP04136 where the reference vaules are gradualy 99.4,99.13,99.80,99.85,99.24,98.53. Considering that highest ANI cut off value of Citrobacter species HSTU-ABK 15 with *Citrobacter amalonaticus* strain CA71 as indicating 99.85%. Also, all the values are showing high similarity with others reference genome as all showed 81% or above ANI value. Here the lowest value was 81.75 with refer to CP024677.1 *Citrobacter freundii* strain UMH. **Table 3** showed the all results of ANI.

Table 3a. Average nucleotide identity (ANIb) of *Citrobacter* sp. strain HSTU-ABk15.

	Citrobacter_sp._HSTU-ABk15	CP011132.1_Citrobacter_amalonaticus_Y19	CP014015.2_Citrobacter_amalonaticus_strain_FDAARGOS_122	CP014070.2_Citrobacter_amalonaticus_strain_FDAARGOS_165	CP022273.1_Citrobacter_freundii_strain_18-1	CP024677.1_Citrobacter_freundii_strain_UMH16	CP044098.1_Citrobacter_portucalensis_strain_FDAARGOS_617	CP044101.1_Citrobacter_werkmanii_strain_FDAARGOS_616	CP057150.1_Citrobacter_sp._RHB35-C17	CP057632.1_Citrobacter_sp._RHB20-C15	CP064180.1_Citrobacter_amalonaticus_strain_CA71	LORU02000001.1_Citrobacter_amalonaticus_strain_FDAARGOS_166	NZ_CP022049.2_Citrobacter_braakii_strain_FDAARGOS_290	NZ_CP039327.1_Citrobacter_portucalensis_strain_Effluent_1	CP041362.1_Citrobacter_amalonaticus_strain_133355.
*Citrobacter*_sp._HSTU-ABk15	*	91.52	95.07	99.13	81.78	81.73	81.93	81.84	99.09	99.87	99.85	98.74	81.82	81.89	99.19
CP011132.1_*Citrobacter_amalonaticus*_Y19	91.26	*	91.95	91.27	81.83	81.29	81.63	81.41	91.30	91.26	91.24	91.47	81.76	81.47	91.27
CP014015.2_*Citrobacter_amalonaticus*_strain_FDAARGOS_122	94.99	92.21	*	94.88	81.93	81.96	81.99	82.02	95.00	94.96	94.93	95.05	82.16	82.02	95.02
CP014070.2_*Citrobacter_amalonaticus*_strain_FDAARGOS_165	99.04	91.52	94.87	*	81.85	81.59	81.87	81.82	98.95	98.87	98.87	98.70	82.03	81.79	99.09
CP022273.1_*Citrobacter_freundii*_strain_18-1	81.81	81.86	81.94	81.97	*	98.23	93.97	90.27	81.84	81.84	81.77	82.23	92.10	94.16	81.83
CP024677.1_*Citrobacter_freundii*_strain_UMH16	81.75	81.73	81.98	81.69	98.31	*	93.96	90.31	81.82	81.85	81.83	81.97	92.04	93.84	81.86
CP044098.1_*Citrobacter_portucalensis*_strain_FDAARGOS_617	81.92	81.83	81.99	81.80	93.78	94.01	*	90.23	81.86	81.79	81.68	81.86	92.29	97.85	81.83
CP044101.1_*Citrobacter_werkmanii*_strain_FDAARGOS_616	81.88	81.66	81.98	81.87	90.27	90.33	90.24	*	81.86	81.88	81.93	81.91	90.41	90.55	81.87
CP057150.1_*Citrobacter*_sp._RHB35-C17	99.13	91.66	95.10	99.11	81.84	81.78	81.82	81.81	*	99.03	99.02	98.79	81.91	81.86	99.11
CP057632.1_*Citrobacter*_sp._RHB20-C15	99.80	91.47	95.04	98.94	81.85	81.88	81.84	81.99	99.03	*	99.66	98.62	81.95	82.05	99.20
CP064180.1_*Citrobacter_amalonaticus*_strain_CA71	99.85	91.59	95.03	99.00	81.81	81.72	81.76	81.84	98.93	99.66	*	98.70	81.86	81.94	99.19
LORU02000001.1_*Citrobacter_amalonaticus*_strain_FDAARGOS_166	98.53	91.57	94.92	98.59	82.15	81.95	81.85	81.93	98.57	98.48	98.51	*	82.03	81.94	98.59
NZ_CP022049.2_*Citrobacter_braakii*_strain_FDAARGOS_290	81.95	82.02	82.08	82.09	92.17	92.16	92.22	90.53	81.96	81.95	81.94	82.10	*	92.12	81.91
NZ_CP039327.1_*Citrobacter_portucalensis*_strain_Effluent_1	81.94	81.88	82.13	81.97	94.01	93.98	97.85	90.66	81.99	82.07	82.04	82.17	92.22	*	81.98
CP041362.1_*Citrobacter_amalonaticus*_strain_133355	99.24	91.59	95.09	99.23	81.86	81.84	81.89	81.90	99.11	99.25	99.21	98.78	81.89	81.99	*

3.4. digital DNA-DNA hybridization (dDDH) analysis of the strain

dDDH is also another method of determining similarity among bacterial species, by cheaking genome to genome distance. Here in table below the dDDH% value proved that, examined species *Citobacter* sp. HSTU-ABk15 showed highest value in formula 1 which is 99.6% with reference species CP057632.1 and also with the same strain in formula 2 and formula 3 again it showed highest value 95.6% and 97.6 thus, they are more similar among all the reference species showed in resulting table. Further searching formula 1, 2 and 3 we have found that *Citobacter sp.* HSTU ABK15 with comparing strain CP 022273.1 showed lowest value as 44.2%, 25.3% and 38.1%. Therefore, it is predicted that these two comparing strains showed less similar than another bacterial genome present in **Table 3b**.

Table 3b. Digital DNA–DNA hybridization (dDDH) for species determination of *Citrobacter* sp. strain HSTU-ABk15.

Subject strain	dDDH (d0, in %)	C.I. (d0, in %)	dDDH (d4, in %)	C.I. (d4, in %)	dDDH (d6, in %)	C.I. (d6, in %)	G+C content difference (in %)
Citrobacter amalonaticus NCTC 10805	89.8	[86.6 -92.4]	93.5	[91.7 -95.0]	92.9	[90.6 -94.7]	0.05
Citrobacter telavivensis 6105	68.9	[65.0 -72.6]	45.7	[43.2 -48.3]	65.0	[61.7 -68.3]	0.09
Citrobacter farmeri DSM 17655	79.9	[75.9 -83.3]	44.2	[41.7 -46.8]	73.2	[69.8 -76.4]	0.02
Citrobacter rodentium NBRC 105723	48.7	[45.2 -52.1]	28.4	[26.0 -30.9]	42.5	[39.5 -45.5]	1.27
Citrobacter sedlakii NBRC 105722	61.6	[57.9 -65.2]	27.8	[25.5 -30.3]	51.1	[48.0 -54.1]	1.34
Citrobacter diversus NCTC 10849	48.4	[45.0 -51.8]	27.1	[24.7 -29.6]	41.7	[38.8 -44.8]	0.21
Citrobacter koseri NCTC 10786	50.2	[46.7 -53.6]	26.8	[24.4 -29.2]	42.8	[39.8 -45.8]	0.43
Levinea malonatica NCTC 10810	49.7	[46.3 -53.2]	26.8	[24.5 -29.3]	42.5	[39.6 -45.6]	0.41
Citrobacter werkmanii NBRC 105721	47.8	[44.4 -51.3]	25.1	[22.8 -27.6]	40.4	[37.4 -43.4]	1.3
Citrobacter youngae CCUG 30791	46.8	[43.4 -50.2]	25.1	[22.8 -27.6]	39.7	[36.7 -42.8]	1.58
Salmonella typhimurium ATCC 13311	37.8	[34.4 -41.3]	24.8	[22.5 -27.2]	33.4	[30.5 -36.5]	1.26
Salmonella typhi NCTC 8385	37.0	[33.6 -40.5]	24.8	[22.5 -27.2]	32.9	[29.9 -36.0]	1.29
Salmonella enterica LT2	37.2	[33.9 -40.7]	24.8	[22.4 -27.2]	33.0	[30.1 -36.1]	1.14
Salmonella enteritidis ATCC 13076	38.2	[34.9 -41.7]	24.7	[22.4 -27.2]	33.7	[30.8 -36.8]	1.24
Salmonella choleraesuis DSM 14846	37.3	[33.9 -40.8]	24.6	[22.3 -27.1]	33.0	[30.1 -36.1]	1.24
Kosakonia oryzendophytica REICA_082	26.8	[23.4 -30.4]	21.6	[19.4 -24.0]	24.6	[21.7 -27.7]	0.35

3.5. Whole genome and housekeeping genes phylogenetic tree of the strain

The phylogenetic tree investigation depended on entire genome groupings of identified *Citrobacter* sp. HSTU-ABk15 detaches from rice shoot and with other 30 genome **(Figure 2A).** Comparison genomes are gathered from NCBI, is a public database Gene Bank. The level of repeat trees in which the related taxa bunched together in the bootstrap test (1000 recreates) is displayed close to the branches. The examined strains *Citobacter* sp. HSTU-ABk15 is showed very similar connection with two groups are – CP 064180.1 *Citobacter amalonaticus* strain CA 71 and CP 057632.1 *Citrobacter* sp. RHB –C15, as they construct monophyletic group (**Figure 2A**). Therefore, it is suggested that *Citobacter* sp. HSTU-ABk15, CP 064180.1 *Citobacter amalonaticus* strain CA 71 and CP 057632.1 *Citobacter* sp. RHB – C15 are derived from same ancestor. The phylogenomic relationship analysis of the housekeeping genes of the strains with their nearest homologs revealed that the *rec*A gene of strain *Citrobacter* sp. HSTU-ABk15 clustered with the *rec*A genes of strains, *Citrobacter amalonaticus* FDAARGOS165, *Citrobacter amalonaticus* CA71, and *Citrobacter* sp. RHB20-C15 with 41% similarity (**Figure 2B**). Furthermore, the *gyr*B gene of *Citrobacter* sp. HSTU-ABk15 clustered the *gyr*B gene of strains *Citrobacter amalonaticus* FDAARGOS165, *Citrobacter amalonaticus* FDAARGOS166, and *Citrobacter* sp. RHB20-C175 demonstrating up to 97% similarity (**Figure 2C**). Conversely, the *gyr*B gene of HSTU-ABk15 paired with *Citrobacter amalonaticus* FDAARGOS122 at a sister node with 77% similarity. The *rpo*B gene of *Citrobacter* sp. HSTU-ABk15 associated with the *rpo*B gene of *Citrobacter amalonaticus* CA71 and *Citrobacter* sp. RHB20-C15 (**Figure 2D**). These findings suggested that *Citrobacter* sp. HSTU-ABk15 is most closely related to *Citrobacter amalonaticus* FDAARGOS166, with notable genetic distances among their nearest homologs in the databases (**Figure 2D**). The 16S rRNA gene sequence analysis also confirmed the strain were not placed in the same node/cluster and deviated from its nearest homologs (*Citrobacter werkmanii* NBRC105721) into a separate cluster (**Figure 2E**).

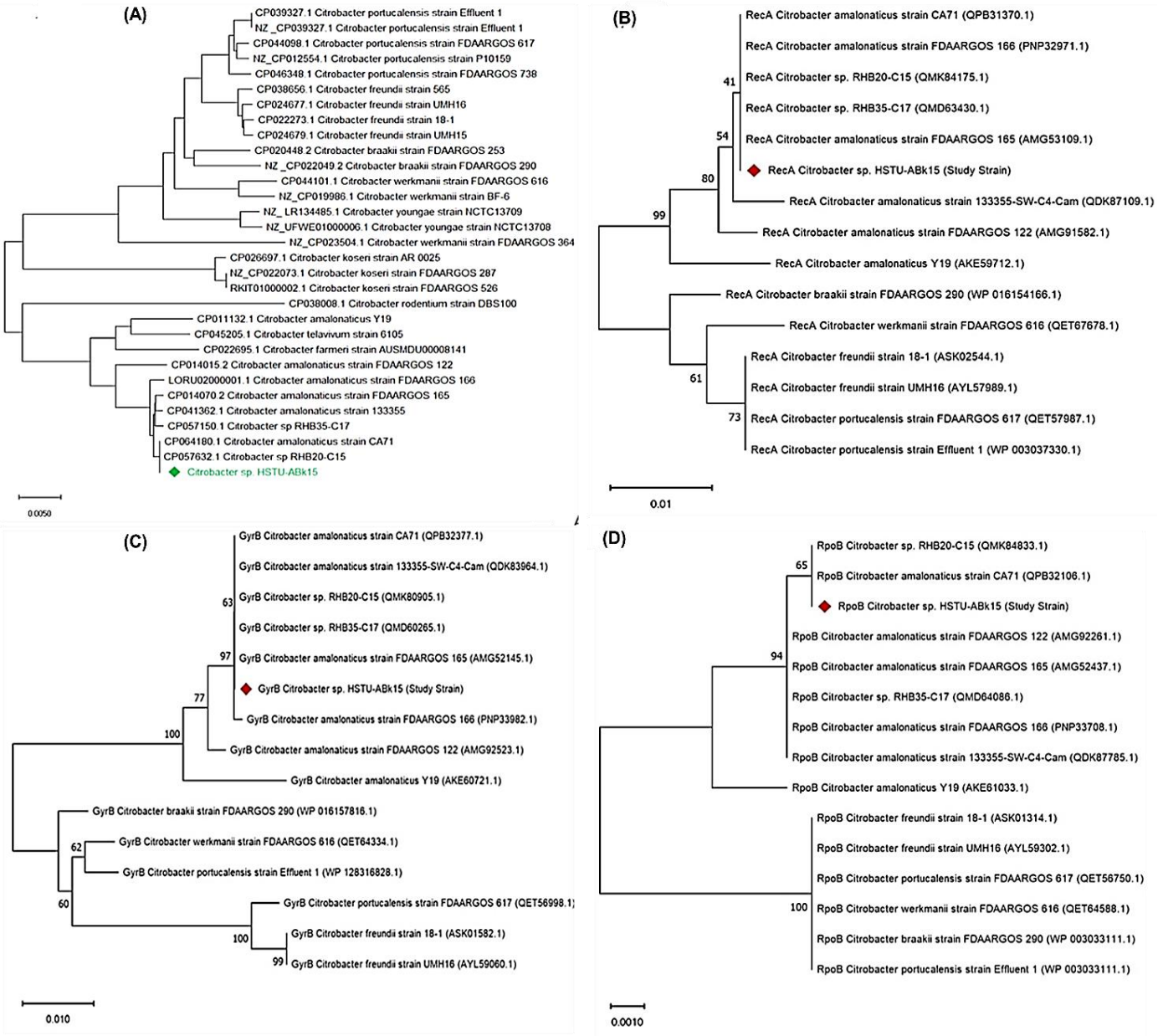
(A)
CP039327.1 Citrobacter portucalensis strain Effluent 1
NZ _CP039327.1 Citrobacter portucalensis strain Effluent 1
CP044098.1 Citrobacter portucalensis strain FDAARGOS 617
NZ_CP012554.1 Citrobacter portucalensis strain P10159
CP046348.1 Citrobacter portucalensis strain FDAARGOS 738
CP038656.1 Citrobacter freundii strain 565
CP024677.1 Citrobacter freundii strain UMH16
CP022273.1 Citrobacter freundii strain 18-1
CP024679.1 Citrobacter freundii strain UMH15
CP020448.2 Citrobacter braakii strain FDAARGOS 253
NZ _CP022049.2 Citrobacter braakii strain FDAARGOS 290
CP044101.1 Citrobacter werkmanii strain FDAARGOS 616
NZ_CP019986.1 Citrobacter werkmanii strain BF-6
NZ_ LR134485.1 Citrobacter youngae strain NCTC13709
NZ_UFWE01000006.1 Citrobacter youngae strain NCTC13708
NZ_CP023504.1 Citrobacter werkmanii strain FDAARGOS 364
CP026697.1 Citrobacter koseri strain AR 0025
NZ_CP022073.1 Citrobacter koseri strain FDAARGOS 287
RKIT01000002.1 Citrobacter koseri strain FDAARGOS 526
CP038008.1 Citrobacter rodentium strain DBS100
CP011132.1 Citrobacter amalonaticus Y19
CP045205.1 Citrobacter telavivum strain 6105
CP022695.1 Citrobacter farmeri strain AUSMDU00008141
CP014015.2 Citrobacter amalonaticus strain FDAARGOS 122
LORU02000001.1 Citrobacter amalonaticus strain FDAARGOS 166
CP014070.2 Citrobacter amalonaticus strain FDAARGOS 165
CP041362.1 Citrobacter amalonaticus strain 133355
CP057150.1 Citrobacter sp RHB35-C17
CP064180.1 Citrobacter amalonaticus strain CA71
CP057632.1 Citrobacter sp RHB20-C15
Citrobacter sp. HSTU-ABk15
0.0050
(B)
RecA Citrobacter amalonaticus strain CA71 (QPB31370.1)
RecA Citrobacter amalonaticus strain FDAARGOS 166 (PNP32971.1)
RecA Citrobacter sp. RHB20-C15 (QMK84175.1)
RecA Citrobacter sp. RHB35-C17 (QMD63430.1)
RecA Citrobacter amalonaticus strain FDAARGOS 165 (AMG53109.1)
RecA Citrobacter sp. HSTU-ABk15 (Study Strain)
RecA Citrobacter amalonaticus strain 133355-SW-C4-Cam (QDK87109.1)
RecA Citrobacter amalonaticus strain FDAARGOS 122 (AMG91582.1)
RecA Citrobacter amalonaticus Y19 (AKE59712.1)
RecA Citrobacter braakii strain FDAARGOS 290 (WP 016154166.1)
RecA Citrobacter werkmanii strain FDAARGOS 616 (QET67678.1)
RecA Citrobacter freundii strain 18-1 (ASK02544.1)
RecA Citrobacter freundii strain UMH16 (AYL57989.1)
RecA Citrobacter portucalensis strain FDAARGOS 617 (QET57987.1)
RecA Citrobacter portucalensis strain Effluent 1 (WP 003037330.1)
0.01
(C)
GyrB Citrobacter amalonaticus strain CA71 (QPB32377.1)
GyrB Citrobacter amalonaticus strain 133355-SW-C4-Cam (QDK83964.1)
GyrB Citrobacter sp. RHB20-C15 (QMK80905.1)
GyrB Citrobacter sp. RHB35-C17 (QMD60265.1)
GyrB Citrobacter amalonaticus strain FDAARGOS 165 (AMG52145.1)
GyrB Citrobacter sp. HSTU-ABk15 (Study Strain)
GyrB Citrobacter amalonaticus strain FDAARGOS 166 (PNP33982.1)
GyrB Citrobacter amalonaticus strain FDAARGOS 122 (AMG92523.1)
GyrB Citrobacter amalonaticus Y19 (AKE60721.1)
GyrB Citrobacter braakii strain FDAARGOS 290 (WP 016157816.1)
GyrB Citrobacter werkmanii strain FDAARGOS 616 (QET64334.1)
GyrB Citrobacter portucalensis strain Effluent 1 (WP 128316828.1)
GyrB Citrobacter portucalensis strain FDAARGOS 617 (QET56998.1)
GyrB Citrobacter freundii strain 18-1 (ASK01582.1)
GyrB Citrobacter freundii strain UMH16 (AYL59060.1)
0.010
(D)
RpoB Citrobacter sp. RHB20-C15 (QMK84833.1)
RpoB Citrobacter amalonaticus strain CA71 (QPB32106.1)
RpoB Citrobacter sp. HSTU-ABk15 (Study Strain)
RpoB Citrobacter amalonaticus strain FDAARGOS 122 (AMG92261.1)
RpoB Citrobacter amalonaticus strain FDAARGOS 165 (AMG52437.1)
RpoB Citrobacter sp. RHB35-C17 (QMD64086.1)
RpoB Citrobacter amalonaticus strain FDAARGOS 166 (PNP33708.1)
RpoB Citrobacter amalonaticus strain 133355-SW-C4-Cam (QDK87785.1)
RpoB Citrobacter amalonaticus Y19 (AKE61033.1)
RpoB Citrobacter freundii strain 18-1 (ASK01314.1)
RpoB Citrobacter freundii strain UMH16 (AYL59302.1)
RpoB Citrobacter portucalensis strain FDAARGOS 617 (QET56750.1)
RpoB Citrobacter werkmanii strain FDAARGOS 616 (QET64588.1)
RpoB Citrobacter braakii strain FDAARGOS 290 (WP 003033111.1)
RpoB Citrobacter portucalensis strain Effluent 1 (WP 003033111.1)
0.0010

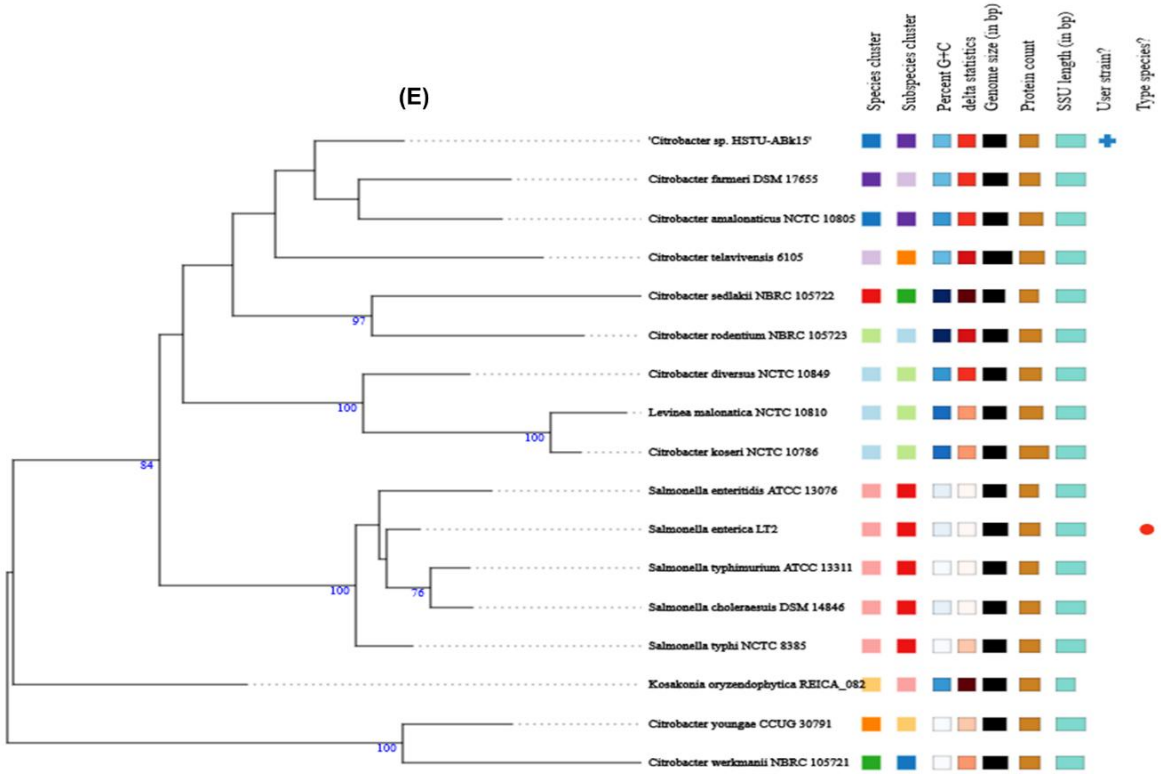

Figure 2. Phylogenetic tree of the strain *Citrobacter* sp. HSTU-ABk15. A) Phylogenetic tree made using A) whole genome sequences B) *rec*A geen, C) *gyr*B gene, D) *rpo*B gene, E) 16S rRNA gene of the strain *Citrobacter* sp. HSTU-Bk15.

3.6. Progressive mauve

The locally collinear squares (LCB) of the genomes of the three nearest strains, specifically *Citrobacter* sp. HSTU-ABk15, CP057632.1 *Citrobacter* sp. RHB 20_C15 and CP064180.1 *Citrobacter amalonaticus* strain CA71, were surveyed using Progressive Mauve **(Figure 3).** Indeed, the LCBs in the genome of *Citrobacter* sp. HSTU ABK 15 are related by lines to similarly tinted LCBs in the genomes of RHB 20_C15, and CA71 strains, independently. The constraints of the LCBs of *Citrobacter* sp. HSTU-ABk15 and various strains taken in assessment are all around considered as breakpoints of genome changes. As shown in Figure, the LCBs of the *Citrobacter* sp. HSTU-ABk15 genome are not really planned with the LCBs of the genomes used for relationship, as shown in Figure. Honestly, a piece of the light blue-tinted LCB of the *Citrobacter* sp. HSTU-ABk15 genome is eradicated, which has displayed in various genomes. So, it recommends that *Citrobacter* sp. HSTU-ABk15, strain is much differed from its closest strains, which demonstrates its transformative properties.

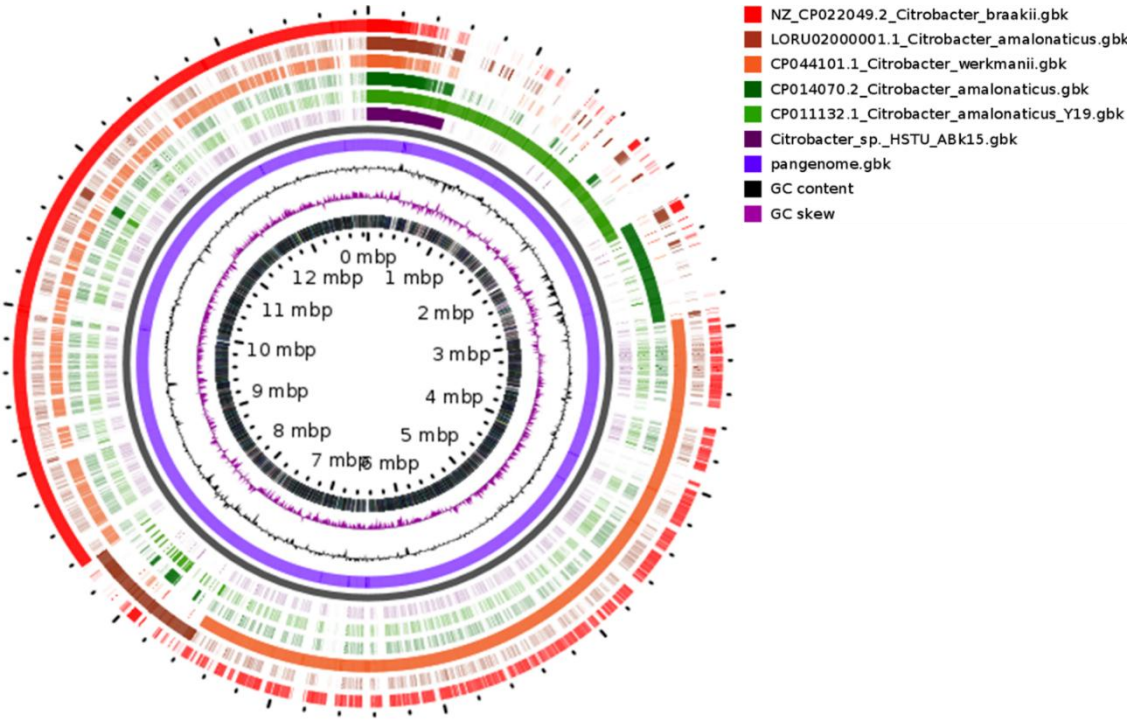

Figure 3. Circular comparative genome map of *Citrobacter* species showing whole-genome alignment of the study strain (*Citrobacter* sp. HSTU-ABK15) against reference *Citrobacter* genomes. From outer to inner rings: annotated CDS on forward and reverse strands, conserved genomic regions among compared genomes, GC content, and GC skew. Genome size is indicated in megabase pairs (Mbp).

3.7. Pangenome analysis

Pangenome analysis process represents entire set of genes from all strains in a legitimate way. The arrangement of the entire genome of *Citrobacter* sp. HSTU ABK 15 with other close to explicit strains, is Visualized by purple tone (short area) (**Figure 4**). Right side of Bottom in the diagram is limited the center genome family's presents within clades of examined and referenced bacterial strains. On other hand, the middle part represents the number of shell genome of these strains. The GC skew is seen in neighborhood genomic districts essentially presented by RNA amalgamation, however the generally genomic extremity because of replication is available no matter what these nearby impacts, and the GC slant is in this way seen in intragenic locales as well as in the third nucleotide positions in codons. Since a couple ori quality and end positions had been distinguished by trial implies, examination of GC slant was first utilized for the computational expectation of ori and ter positions in genome successions.

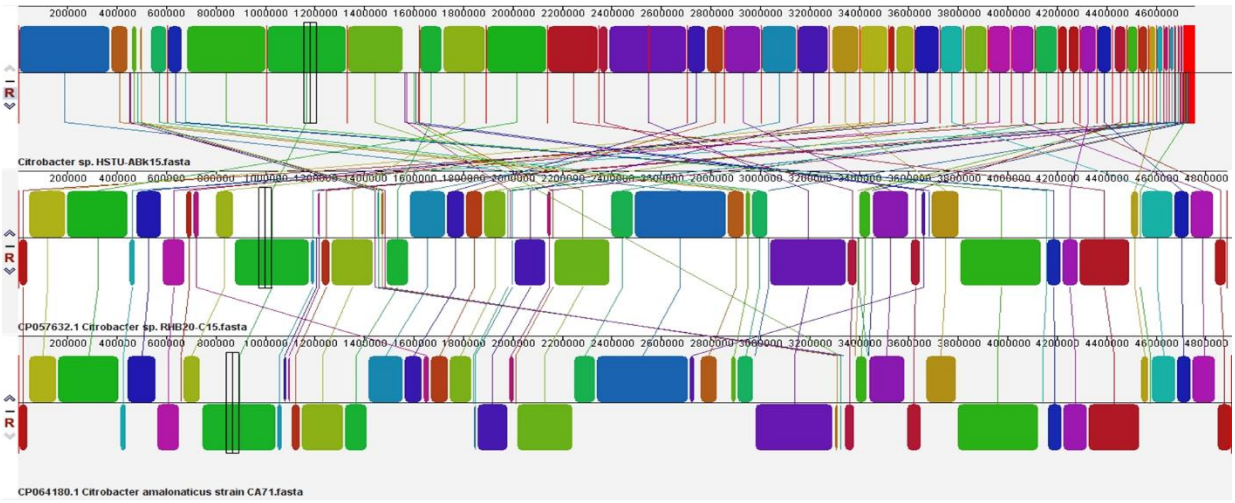

Figure 4. Progressive Mauve alignment (LCBs) of the strain Citrobacter sp. HSTU-ABk15 with their nearest homologs.

3.8. Abundance plant growth promoting genes

In the genome of *Citrobacter* sp. HSTU-ABk15 nitrogen fixation gene (nif JSUL,iscUAR) are annotated (**Table 4a**). Moreover, nitrosative stress tolerance gene norR,nsrR,glnK etc,nitrogen metabolism regulatory protein glnD, glnB, pstN, Siderophores (fes, entFS, and fepA) are plant hormones, phosphate metabolism, biofilm formation, root colonization, sulfur detection and metabolism, which contribute to the development of plant growth, were identified.Acc deaminase producing gene dcyD, rimM, vital IAA producing gene trpCF, trpABSD, pitA, pstSCAB, phoUAEBR, pnt AB, ppx, ppk1. Additionally, vital genes for producing chemotaxins,motility, adhesive structure, trehalose metabolism in plant are also identify in the experimental genome sequence. Therefore, this study examined almost all aspects of PGP such as nitrogen fixation, IAA, siderophore, phosphate, ACC, HCN, and ammonia production in this study, *Citobacter* sp. HSTU-ABK 15 isolates showed positive siderophore production. Siderophore production by these species anticipates the importance of plant nutrients in mature ripening conditions in iron-rich conditions. The gene showed the strong activity of siderophore and the biosynthesis method of siderophore (fes, entFS, and fepA) was also observed in its genome study.

Table 4a. Genes associated with PGP traits *Citrobacter* sp. strain HSTU-ABk15.

PGP activities description	Gene Name	Gene annotation	Chromosome location	Locus Tag (HSTU	E.C. number
Nitrogen fixation	nifJ	Pyruvate: ferredoxin (flavodoxin) oxidoreductase	89885..93409	GN159_00425	-
	nifE	nitrogenase iron-molybdenum cofactor biosynthesis protein			-
	nifH	nitrogenase iron protein			1.18.6.1
	nifA	nif-specific transcriptional activator			-
	nifB	nitrogenase cofactor biosynthesis protein			-
	nifM	nitrogen fixation protein			-
	nifS	cysteine desulfurase	80147..81361	GN159_13755	2.8.1.7
	nifU	Fe-S cluster assembly protein			-
	nifN	nitrogenase iron-molybdenum cofactor biosynthesis protein			-
	nifT	putative nitrogen fixation protein			-
	nifK	nitrogenase molybdenum-iron protein subunit beta			1.18.6.1
	nifV	homocitrate synthase			2.3.3.14
	iscU	Fe-S cluster assembly scaffold	79735..80121	GN159_13750	-

	iscA	Fe-S cluster assembly protein	79392..79715	GN159_13745	-
	iscR	Fe-S cluster assembly transcriptional regulator	81597..82088	GN159_13760	-
	nifL	Nitrogen fixation negative regulator			-
Nitrosative stress	norR	nitric oxide reductase transcriptional regulator	71118..72635	GN159_15825	-
	nsrR	Nitric oxide sensing transcriptional repressor	21715..22140	GN159_20345	-
	ntrB	Nitrate ABC transporter			-
	glnK	P-II family nitrogen regulator	167620..167958	GN159_08475	-
	norV	anaerobic nitric oxide reductase flavorubredoxin	72823..74268	GN159_20345	-
Nitrogen metabolism regulatory protein	glnD	Bifunctional uridylyl removing protein	35056..37728	GN159_04990	2.7.7.59
	glnB	Nitrogen regulatory protein P-II	105885..106223	GN159_13860	-
	ptsN	Nitrogen regulatory protein PtsN	71533..72024		-
Ammonia assimilation	gltB	glutamate synthase large subunit	59432..63892	GN159_17450	1.4.1.13
	gltS	sodium/glutamate symporter	52826..54031	GN159_16320	
	amtB	Ammonium transporter AmtB	166302..167588	"GN159_08470	-
Nitrate reductase, nitrite reductase and associated transporters	-	nitrate reductase subunit alpha	222272..226015	GN159_01070	1.7.99.4
	*nar*H	nitrate reductase subunit beta	220740..222275	GN159_01065	1.7.99.4
	*nar*J	nitrate reductase molybdenum cofactor assembly chaperone	220033..220743	GN159_01060	-
	*nar*I	respiratory nitrate reductase subunit gamma	219356..220033	GN159_01055	1.7.99.4
	*Nir*D	nitrite reductase small subunit NirD	223444..223770	GN159_09940	-
	*nap*A	nitrate reductase catalytic subunit NapA	5160..7646	GN159_12040	-
	*nap*B	nitrate reductase cytochrome c-type subunit	9195..9644	GN159_12055	1.9.6.1
ACC deaminase	dcyD	D-cysteine desulfhydrase	436619..437605	GN159_02115	4.4.1.15
	rimM	ribosome maturation factor RimM	43700..44248	GN159_21015	-
Siderophore					
Siderophore enterobactin	fes	enterochelin esterase	20211..21419	GN159_07885	3.1.1.-
	entF	enterobactin non-ribosomal peptide synthetase EntF	16069..19965	GN159_07875	6.3.2.14
	entC	isochorismate synthase EntC	8204..9379	GN159_07840	5.4.4.2
	entS	enterobactin transporter EntS	10552..11790	GN159_07850	-
	entE	2,3-dihydroxybenzoyl)adenylate synthase	6587..8194	GN159_07835	2.7.7.58
	entD	enterobactin synthase subunit EntD	23982..24605	GN159_07895	6.3.2.14
	entH	proofreading thioesterase EntH	4545..4958	GN159_07820	3.1.2.-
	fhuA	ferrichrome porin FhuA	52979..55231	GN159_05065	-
	fhuB	Fe (3^+)-hydroxamate ABC transporter permease FhuB	49265..51247	GN159_05050	-
	fhuC	$Fe3^+$-hydroxamate ABC transporter ATP-binding protein	52134..52931	GN159_05060	-
	fhuD	Fe (3^+)-hydroxamate ABC transporter substrate-binding protein	51244..52134	GN159_05055	-
	fhuF	Siderophore iron reductase	155146..155934	GN159_03720	-
	tonB	TonB system transport protein TonB	196254..196970	GN159_00930	-
	fepB	$Fe2^+$-enterobactin ABC transporter substrate-binding protein	9564..10502	GN159_07845	-
	fepG	iron-enterobactin ABC transporter permease	12903..13895	12903..13895	-
	exbD	TonB system transport protein ExbD	85669..86094	GN159_17055	-
	-	TonB family protein			-
	-	ABC transporter substrate-binding protein	97798..98715	GN159_15950	-
	rpoA	DNA-directed RNA polymerase subunit alpha	11226..12215	GN159_21745	2.7.7.6
	rpoB	DNA-directed RNA polymerase subunit beta	24571..28599	GN159_21625	2.7.7.6
	exbB	tol-pal system-associated acyl-CoA thioesterase	84928..85662	GN159_17050	-
Plant hormones					
IAA production	trpCF	bifunctional indole-3-glycerol-phosphate synthase TrpC	183231..184589	GN159_00860	4.1.1.48/5.3.1.24
	trpS	tryptophan--tRNA ligase	219626..220630	GN159_09920	6.1.1.2
	trpA	tryptophan synthase subunit alpha	185793..186599	GN159_00870	4.2.1.20
	trpB	tryptophan synthase subunit beta	184600..185793	GN159_00865	4.2.1.20
	trpD	bifunctional anthranilate synthase glutamate amido transferase component	181632..183227	GN159_00855	2.4.2.18/4.1.3.27
Phosphate metabolism	pitA	inorganic phosphate transporter PitA	92676..94175	GN159_09340	-
	pstS	phosphate ABC transporter substrate-binding protein PstS	57255..58295	GN159_20100	-
	pstC	phosphate ABC transporter permease PstC	56103..57062	GN159_20095	-
	pstA	phosphate ABC transporter permease PstA	55213..56103	GN159_20090	-
	pstB	phosphate ABC transporter ATP-binding protein PstB	54342..55142	GN159_20085	-
	phoU	phosphate signaling complex protein PhoU	53592..54317	GN159_20080	3.5.2.6

	ugpB	sn-glycerol-3-phosphate ABC transporter substrate-binding protein UgpB	144375..145691	GN159_09600	--
	ugpE	sn-glycerol-3-phosphate ABC transporter substrate-binding protein UgpE	145798..146685	GN159_09605	-
	phoA	alkaline phosphatase	255735..257150	GN159_08885	3.1.3.1
	phoE	phosphoporin PhoE	4235..5287	GN159_22245	-
	phoB	phosphate response regulator transcription factor PhoB	243156..243845	GN159_08820	-
	phoR	phosphate regulon sensor histidine kinase PhoR	241819..243114	GN159_08815	2.7.13.3
	ppx	exopolyphosphatase	44189..45730	GN159_13610	3.6.1.11
	ppk1	polyphosphate kinase 1	42118..44184	GN159_13605	2.7.4.1
	phoH	phosphate starvation-inducible protein PhoH	77077..77985	GN159_15210	-
	pntA	Re/Si-specific NAD(P)(+) transhydrogenase subunit alpha	21952..23340	GN159_06365	1.6.1.2
	pntB	Re/Si-specific NAD(P)(+) transhydrogenase subunit beta"	21952..23340	GN159_06365	-
	phoQ	two-component system sensor histidine kinase PhoQ	17911..19374	GN159_21970	2.7.13.3
	tomB	Hha toxicity modulator TomB	156839..157213	GN159_08395	-
Biofilm formation	luxS	S-ribosylhomocysteine lyase	54902..55417	GN159_15720	4.4.1.21
	murJ	Murein biosynthesis integral membrane protein MurJ	44743..46278	GN159_15010	-
	flgH	Flagellar basal body L-ring protein FlgH	37858..38556	GN159_14960	-
	flgJ	Flagellar assembly peptidoglycan hydrolase FlgJ	35798..36748	GN159_14950	3.2.1.-
	flgK	Flagellar hook-associated protein FlgK	34098..35732	GN159_14945	-
	flgL	Flagellar hook-filament junction protein FlgL	33130..34083	GN159_14940	-
	flgM	Flagellar biosynthesis anti-sigma factor FlgM	43934..44227	GN159_15000	-
	flgA	Flagellar basal body P-ring formation protein	43184..43840	GN159_14995	-
	flgB	Flagellar basal body rod protein FlgB	42611..43027	GN159_14990	-
	flgC	Flagellar basal body rod protein FlgC	42203..42607	GN159_14985	-
	flgI	Flagellar basal body P-ring protein FlgI	36748..37845	GN159_14955	-
	flgG	Flagellar basal-body rod protein FlgG	38614..39396	GN159_14965	-
	motA	Flagellar motor stator protein MotA	403908..404801	GN159_01925	-
	motB	Flagellar motor protein MotB	402982..403911	GN159_01920	-
	efp	elongation factor P	199268..199834	199268..199834	-
	hfq	RNA chaperone Hfq	15692..16000	GN159_20315	-
Sulfur assimilation and metabolism	cysZ	sulfate transporter CysZ	13096..13857	GN159_21180	-
	cysK	cysteine synthase A	14021..14992	GN159_21185	2.5.1.47
	cysM	cysteine synthase CysM	21306..22217	GN159_21230	2.5.1.47
	cysA	sulfate/thiosulfate ABC transporter ATP-binding protein CysA	22327..23421	GN159_21235	-
	cysW	sulfate/thiosulfate ABC transporter permease CysW"	23411..24286	GN159_21240	-
	cysC	adenylyl-sulfate kinase	113797..114402	GN159_16040	2.7.1.25
	cysN	sulfate adenylyl transferase subunit CysN	114402..115829	GN159_16045	2.7.7.4
	cysD	sulfate adenylyl transferase subunit CysD	115839..116747	GN159_16050	2.7.7.4
	cysH	Phosphor adenosine phosphosulfate reductase	118125..118859	GN159_16060	1.8.4.8
	cysI	assimilatory sulfite reductase (NADPH)	118918..120630	GN159_16065	1.8.1.2
	cysJ	NADPH-dependent assimilatory sulfite reductase flavoprotein subunit	120630..122429	GN159_16070	1.8.1.2
	cysT	sulfate/thiosulfate ABC transporter permease CysT	24286..25119	GN159_21245	-
	cysE	serine O-acetyltransferase	96590..97411	GN159_16540	2.3.1.30
	cysQ	3'(2'),5'-bisphosphate nucleotidase CysQ	42762..43502	GN159_20460	3.1.3.7
	cysK	cysteine synthase A	14021..14992	GN159_21185	2.5.1.47
	cysS	cysteine--tRNA ligase	101698..103083	GN159_08160	6.1.1.16
	fdxH	formate dehydrogenase subunit beta	66311..67195	GN159_19720	-
Antimicrobial peptide	pagP	lipid IV(A) palmitoyltransferase PagP	19072..19650	GN159_14155	2.3.1.251
	sapC	peptide ABC transporter permease SapC	150822..151712	GN159_00715	-
	sapB	peptide ABC transporter permease SapB	149870..150835	GN159_00710	-
	lipA	lipoyl synthase	21780..22745	GN159_14180	2.8.1.8
	lipB	lipoyl(octanoyl) transferase LipB	24206..24847	GN159_14190	2.3.1.181
	amyA	alpha-amylase	GN159_02155	444158..445645	3.2.1.1
Synthesis of resistance inducers					
Methanethiol	metH	methionine synthase	8358..12041	GN159_10125	2.1.1.13
2,3-butanediol	ilvB	acetolactate synthase large subunit	10737..12431	GN159_19875	-

	ilvN	acetolactate synthase small subunit	10443..10733	GN159_19870	2.2.1.6
	ilvA	Serine, threonine dehydratase	83915..85459	GN159_19345	4.3.1.19
	ilvC	ketol-acid reductoisomerase	73955..75430	GN159_19305	1.1.1.86
	ilvY	HTH-type transcriptional activator IlvY	75589..76491	GN159_19310	-
	ilvD	Dihydroxy-acid dehydratase	85462..87312	GN159_19350	4.2.1.9
	ilvM	acetolactate synthase 2 small subunits	88322..88585	GN159_19360	2.2.1.6
isoprene	idi	isopentenyl-diphosphate Delta-isomerase	206722..207270	GN159_03980	5.3.3.2
	gcpE/ ispG	flavodoxin-dependent (E)-4-hydroxy-3-methylbut-2-enyl-diphosphate synthase	61021..62139	GN159_13680	1.17.7.1
	ispE	4-(cytidine 5'-diphospho)-2-C-methyl-D-erythritol kinase	241790..242641	GN159_01155	2.7.1.148
Spermidine	*spe*E	Polyamine aminopropyltransferase	78192..79058	GN159_05175	2.5.1.16
synthesis	*spe*A	biosynthetic arginine decarboxylase	267633..269609	GN159_06005	4.1.1.19
	*spe*B	agmatinase	266569..267489	GN159_06000	3.5.3.11
	*spe*D	adenosylmethionine decarboxylase	79074..79868	GN159_05180	4.1.1.50
nitrate reductase,	-	nitrate reductase subunit alpha	222272..226015	GN159_01070	1.7.99.4
nitrite reductase	*nar*H	nitrate reductase subunit beta	220740..222275	GN159_01065	1.7.99.4
and	*nar*J	nitrate reductase molybdenum cofactor assembly chaperone	220033..220743	GN159_01060	-
associated transporters	*nar*I	respiratory nitrate reductase subunit gamma	219356..220033	GN159_01055	1.7.99.4
	*Nir*D	nitrite reductase small subunit NirD	223444..223770	GN159_09940	-
	*nap*A	nitrate reductase catalytic subunit NapA	5160..7646	GN159_12040	-
	*nap*B	nitrate reductase cytochrome c-type subunit	9195..9644	GN159_12055	1.9.6.1
Symbiosis-related	gcvR	glycine cleavage system transcriptional repressor	26311..26949	GN159_13530	-
	pyrC	dihydroorotase	51561..52607	GN159_15045	3.5.2.3
	gcvT	glycine cleavage system aminomethyltransferase	188966..190060	GN159_03895	2.1.2.10
	phnC	phosphonate ABC transporter ATP-binding protein	121787..122575	GN159_10630	-
	tatA	Sec-independent protein translocasesubunit TatA	12862..13131	GN159_19015	-
	bacA	undecaprenyl-diphosphate phosphatase	46469..47290	GN159_16875	3.6.1.27
	zur	Transcriptional repressor /zinc uptake transcriptional repressor	62145..62660	GN159_10355	-
Oxidoreductase	sodB	superoxide dismutase [Fe]	75750..76331	GN159_06615	1.15.1.1
	gpx	glutathione peroxidase	149085..149636	GN159_06975	1.11.1.9
	osmC	peroxiredoxin OsmC	59451..59882	GN159_19680	1.11.1.15
Hydrolase	ribA	GTP cyclohydrolase II	165668..166258	GN159_00790	3.5.4.25
	folE	GTP cyclohydrolase I FolE	58055..58723	GN159_12285	3.5.4.16
	bglX	beta-glucosidase BglX	82930..85227	GN159_12410	3.2.1.21
	malZ	maltodextrin glucosidase	236687..238504	GN159_08800	3.2.1.20
	bglA	6-phospho-beta-glucosidase	38561..39991	GN159_13590	3.2.1.86
	-	chitinase			-
	gdhA	NADP-specific glutamate dehydrogenase	193575..194918	GN159_07215	1.4.1.4
	-	cellulase	60128..61237	N159_09220	3.2.1.4
	amyA	alpha-amylase	444158..445645	GN159_02155	3.2.1.1
Root colonization					
Chemotaxis	malE	maltose/maltodextrin ABC transporter substrate-binding protein	49812..51002	GN159_10300	-
	cheY	Two-component system response regulator/ chemotaxis protein CheY	393087..393476	GN159_01880	-
	cheB	chemotaxis-specific protein-glutamate methyltransferase CheB	393494..394543	GN159_01885	3.1.1.61
	mcp	methyl-accepting chemotaxis protein	136006..137670	GN159_03625	
	tap	methyl-accepting chemotaxis protein IV	395426..397027	GN159_01895	-
	cheW	chemotaxis protein CheW	400422..400925	GN159_01910	-
	cheA	chemotaxis protein CheA	400947..402977	GN159_01915	-
	rbsB	ribose ABC transporter substrate-binding protein RbsB	83115..84005	GN159_20215	-
Motility	flhA	flagellar biosynthesis protein FlhA	383641..385719	GN159_01845	-
Flagellar	flhB	flagellar type III secretion system protein	385712..386866	GN159_01850	-
components	flhC	Transcriptional activator FlhC/ flagellar transcriptional regulator	404927..405505	GN159_01930	-
	flhD	flagellar transcriptional regulator FlhD	405508..405858	GN159_01935	-
	fliZ	flagella biosynthesis regulatory protein FliZ	438602..439153	GN159_02125	-
	fliD	Flagellar filament capping protein FliD	441889..443295	GN159_02140	-
	fliS	flagellar export chaperone Proein	443311..443718	GN159_02145	-
	fliE	flagellar hook-basal body complex protein FliE	457283..457597	GN159_02235	-

	fliF	flagellar basal body M-ring protein FliF	457814..459508	GN159_02240	-
	fliG	flagellar motor switch protein FliG	459501..460499	GN159_02245	-
	fliT	flagella biosynthesis regulatory protein FliT	443718..444089	GN159_02150	
	fliH	flagellar assembly protein FliH	460492..461196	GN159_02250	-
	fliL	flagellar basal body-associated protein FliL	464344..464808	GN159_02270	-
	fliM	flagellar motor switch protein FliM	464813..465817	GN159_02275	-
	fliP	Flagellar biosynthetic protein FliP/flagellar type III secretion system pore protein	466604..467341	GN159_02290	-
	fliQ	flagellar biosynthesis protein FliQ	467351..467620	GN159_02295	-
	*flg*K	flagellar hook-associated protein FlgK	323454..325103	GPJ58_01465	-
	*fli*D	flagellar filament capping protein FliD	345803..347203	GPJ58_01580	-
Adhesive structure	hofC	protein transport protein HofC	106592..107794	GN159_05290	-
Adhesin production	PgaA	poly-beta-1,6 N-acetyl-D-glucosamine export porin PgaA			-
	pgaB	poly-beta-1,6-N-acetyl-D-glucosamine N-deacetylase PgaB			3.5.1.-
	pgaC	poly-beta-1,6 N-acetyl-D-glucosamine synthase			-
	pgaD	poly-beta-1,6-N-acetyl-D-glucosamine biosynthesis protein			-
Superoxide dismutase	sodA	superoxide dismutase [Mn]	83355..83975	GN159_18020	1.15.1.1
	sodB	superoxide dismutase [Fe]	75750..76331	GN159_06615	1.15.1.1
	sodC	superoxide dismutase [Cu-Zn] SodC2	64324..64845	GN159_06565	1.15.1.1
Trehalose metabolism	treB	PTS trehalose transporter subunit IIBC	16145..17563	GN159_03075	2.7.1.201
	treC	alpha,alpha-phosphotrehalase	14439..16097	GN159_03070	3.2.1.93
	treR	HTH-type transcriptional regulator TreR	17709..18656	GN159_03080	
	otsA	alpha,alpha-trehalose-phosphate synthase	407099..408520	GN159_01945	2.4.1.15
	otsB	trehalose-phosphatase	408495..409295	GN159_01950	3.1.3.12
	lamB	maltoporin LamB	52556..53881	GN159_10310	-

3.9. Abundance of abiotic stress tolerance genes

Interestingly, we found stress tolerance gene such as *csp*A, cspD, cspE (for cold shock), heat shock proteins- smpB, hslR, groES, rpoS, (absobingly here we found two class of chaperone protein one group of heat shock chaperone- ibpA, ibpB, hspQ and another group of molecular chaperone–dnaJ, dnaK,djl A), proteins responsible for arsenic tolerance – arsA, arsB, ars C, arsD, arsR, arsH in the genome of *Citobacter* sp. HSTU-ABK 15. Interestingly, the gene associated with drought stress tolerance includes proA, proB,proQ , proX found within the genome of *Citobacter* sp. HSTU-ABk 15. These genes were linked to the modification of drought-induced functions. In addition, genes of copper homeostasis and magnesium copA, copE and copC, copD, *cusR, cus*F, *cusA* were found in the genome of *Citrobacter* sp. HSTU-ABk15 (**Table 4b)**.

Table 4b. Gene associated with stress tolerating *Citrobacter* sp. strain HSTU-ABK15.

Activity description	Gene Name	Gene annotation	Chromosome location (HSTU-ABk15)	Locus Tag (HSTU-ABk15)	E.C. number
Cold Shock protein	*cspA*	RNA chaperone/antiterminator CspA	24474..24686	GN159_09060	-
	cspE	transcription antiterminator/RNA stability regulator CspE	19824..20033	GN159_14160	-
	cspD	cold shock-like protein CspD	146770..146991	GN159_13405	-
Heat Shock protein	*smpB*	SsrA-binding protein SmpB	34197..34679	GN159_20960	-
	hslR	ribosome-associated heat shock protein Hsp15	203743..204144	GN159_09840	
	ibpA	heat shock chaperone IbpA	25153..25566	GN159_19945	-
	ibpB	heat shock chaperone IbpB	24576..25004	GN159_19940	-
	hspQ	heat shock protein HspQ	94338..94655	GN159_18475	-
	groL	chaperonin GroEL	194845..196491	GN159_10970	-
	groES	Heat shock protein 60 family co-chaperone GroES	194508..194801	GN159_10965	-
	yegD	Putative heat shock protein YegD	120266..121618	GN159_12565	
	dnaJ	molecular chaperone DnaJ	216138..217271	GN159_05775	-
	dnaK	molecular chaperone DnaK	217357..219273	GN159_05780	-

	djlA	co-chaperone DjlA	163982..164797	GN159_05535	
	rpoH	RNA polymerase sigma factor RpoH	134729..135583	GN159_09555	-
	lepA	elongation factor 4	130011..131810	GN159_13965	3.6.5.n1
	grpE	nucleotide exchange factor GrpE	38863..39456	GN159_20990	-
Heavy metal resistance					
Arsenic tolerance	*arsA*	arsenical pump-driving ATPase	239306..241057	GN159_04105	-
	arsB	arsenical efflux pump membrane protein ArsB	241105..242394	GN159_04110	-
	arsC	arsenate reductase (glutaredoxin)	242407..242832	GN159_04115	1.20.4.1
	arsD	arsenite efflux transporter metallochaperone ArsD	238926..239288	GN159_04100	
	arsR	metalloregulator ArsR/SmtB family transcription factor	238525..238878	GN159_04095	-
	arsH	Arsenical reseistance protein arsH			-
	acrR	ultidrug efflux transporter transcriptional repressor AcrR	151167..151820	GN159_08380	-
	acrA	Multidrug efflux RND transporter periplasmic adaptor subunit	151962..153155	GN159_08385	-
	acrD	Multidrug efflux RND transporter permease	14279..17392	GN159_13475	-
	trkA	Trk system potassium transporter TrkA	7689..9065	GN159_21715	-
Chromium resistance	*chrA*	Chromate efflux transporter			-
Magnesium transport	*corA*	magnesium/cobalt transporter CorA	31974..32924	GN159_19105	-
	corC	CNNM family magnesium/cobalt transport protein CorC	45543..46421	GN159_14295	-
	cobA	uroporphyrinogen-III C-methyltransferase	221113..222486	GN159_09930	2.1.1.107
Copper homeostasis	*copA*	copper-exporting P-type ATPase CopA	127025..129526	GN159_08285	-
	copC	copper homeostasis periplasmic binding protein CopC			-
	copD	copper homeostasis membrane protein CopD	347230..348102	GN159_01660	-
	cutC	copper homeostasis protein CutC	376921..377667	GN159_01815	
	cusR	copper response regulator transcription factor CusR	84118..84801	GN159_08105	
	cusA	CusA/CzcA family heavy metal efflux RND	77741..80887	GN159_08085	-
	cusF	cation efflux system protein CusF	82194..82538	GN159_08095	-
Zinc homeostasis	*znuA*	zinc ABC transporter substrate-binding protein ZnuA	364902..365846	GN159_01745	-
	znuB	zinc ABC transporter permease subunit ZnuB	366677..367462	GN159_01755	-
	znuC	zinc ABC transporter ATP-binding protein ZnuC	365925..366680	GN159_01750	-
Zinc, cadmium, lead, mercury homeostasis	*zntA*	Zn(II)/Cd(II)/Pb(II) translocating P-type ATPase ZntA	126783..128981	GN159_09515	-
Zinc homeostasis	*adhP*	alcohol dehydrogenase AdhP	95847..97039	GN159_00445	1.1.1.1
	htpX	protease HtpX	335203..336084	GN159_01605	3.4.24.-
	zntB	zinc transporter ZntB	105499..106482	GN159_00490	-
Manganese homeostasis	*mntR*	manganese-binding transcriptional regulator MntR	76576..77049	GN159_13085	-
	mntP	manganese efflux pump MntP	327375..327941	GN159_01555	-
	mntH	Mn (2+) uptake NRAMP transporter MntH	7071..8309	GN159_11090	-
		zinc/cadmium/mercury/lead-transporting ATPase			3.6.3.3
Drought resistance	*nhaA*	Na+/H+ antiporter NhaA	209625..210791	GN159_05750	-
	chaA	sodium-potassium/proton antiporter ChaA	234512..235612	GN159_01115	-
	chaB	putative cation transport regulator ChaB	234008..234238	GN159_01110	-
	proA	glutamate-5-semialdehyde dehydrogenase	6690..7943	GN159_22255	1.2.1.41
	proB	glutamate 5-kinase	5575..6678	GN159_22250	2.7.2.11
	proQ	RNA chaperone ProQ	338345..339031	GN159_01615	-
	proV	glycine betaine/L-proline ABC transporter ATP-binding protein	43418..44620	GN159_15665	-
	proW	glycine betaine/L-proline ABC transporterpermease ProW	44613..45677	GN159_15670	-

	proX	glycine betaine/L-proline ABC transporter substrate-binding protein ProX	45746..46741	GN159_15675	-
	proP	glycine betaine/L-proline transporter ProP	129061..130563	GN159_10660	-
	proS	proline--tRNA ligase	4928..6646	GN159_04850	6.1.1.15
	betA	choline dehydrogenase	39978..41654	GN159_07965	1.1.99.1
	betB	betaine-aldehyde dehydrogenase	38492..39964	GN159_07960	1.2.1.8
	betT	choline BCCT transporter BetT			-
	trkA	Trk system potassium transporter TrkA	7689..9065	GN159_21715	-
	trkH	Trk system potassium transporter TrkH	654..2105	GN159_18960	-
	kdbD	two-component system sensor histidine kinase KdbD	79412..82099	GN159_14470	2.7.13.3
	kdpA	potassium-transporting ATPase subunit KdpA	84741..86420	GN159_14485	-
	*kdp*B	potassium-transporting ATPase subunit KdpB	82673..84721	GN159_14480	-
	*kdp*C	potassium-transporting ATPase subunit KdpC	82089..82664	GN159_14475	-
	*kdp*E	/two-component system response regulator KdpE	78738..79415	GN159_14465	-
	*kdp*F	two-component system response regulator KdpE	86420..86509	GN159_14490	-

3.10. Genes associated with pesticide degradation

Citrobacter sp. HSTU-ABk15 has identified a genetic component that includes the destruction of organophosphorus pesticides. In the genome of HSTU-ABk15 a total number of 22 enzymes were found which are involved in pesticide degrading, where six enzymes are categorized as phosphonate C-P lyase system protein (phn GHIJKL), two genes categorized as cyclic family protein specified in gene annotation in the table no. as cyclic-guanylate-specific phosphodiesterase (pdeH), cyclic di-GMP phosphodiesterase(pdeR). Moreover, in the HSTU-ABk15 genome 1,6-anhydro-N-acetylmuramyl-L-alanineamidase, anaerobic glycerol-3-phosphate dehydrogenase subunit, glycerol-3-phosphate dehydrogenase subunit, Glycerol phosphodiester phosphodiesterase, leucyl aminopeptidase were also observed. In this study, *Citrobacter* sp. HSTU-ABk15 22 different genes that product was suggested to be involved in damaging organophosphorus pesticides (**Table 4c)**.

Table 4c. Genes associated with pesticide degradation available in the genome of *Citrobacter* sp. HSTU-ABk15.

Activity description	Gene Name	Gene annotation	Chromosome location (HSTU-ABk15)	Locus Tag (HSTU-ABk15)	E.C. number
	*amp*D	1,6-anhydro-N-acetylmuramyl-L-alanineamidase	103013..103576	GN159_05270	3.5.1.28
	*glp*A	anaerobic glycerol-3-phosphate dehydrogenase subunit	159935..161563	GN159_11860	1.1.5.3
	*glp*B	glycerol-3-phosphate dehydrogenase subunit	158686..159945	GN159_11855	1.1.5.3
	*glp*Q	Glycerol phosphodiester phosphodiesterase	163200..164276	GN159_11870	3.1.4.46
Pesticide degrading	*pep*A	leucyl aminopeptidase	47850..49361	GN159_03220	3.4.11.1
	*pep*B	aminopeptidase PepB	75048..76331	GN159_13720	3.4.11.23
	*pep*D	cytosol nonspecific dipeptidase	142..1599	GN159_22225	3.4.13.18
	*pep*E	-/dipeptidase PepE	14030..14719	GN159_10135	3.4.13.21
	*phn*F	phosphonate metabolism transcriptional regulator PhnF	118999..119724	GN159_10615	-
	*phn*D	phosphonate ABC transporter substrate-binding protein	120622..121638	GN159_10625	-
	*phn*G	phosphonate C-P lyase system protein PhnG	118546..118998	GN159_10610	-
	*phn*H	phosphonate C-P lyase system protein PhnH	117965..118549	GN159_10605	2.7.8.37

*phn*I	phosphonate C-P lyase system protein PhnI	116898..117965	GN159_10600	-
*phn*J	phosphonate C-P lyase system protein PhnJ	116060..116908	GN159_10595	-
*phn*K	phosphonate C-P lyase system protein PhnK	115305..116063	GN159_10590	-
*phn*L	phosphonate C-P lyase system protein PhnL	114546..115232	GN159_10585	-
*phn*M	Ipha-D-ribose 1-methylphosphonate 5 triphosphatediphosphatase	113413..114549	GN159_10580	3.6.1.63
*phn*P	phosphonate metabolism protein PhnP	111630..112388	GN159_10565	3.1.4.55
phnO	aminoalkylphosphonate N-acetyltransferase	112435..112869	GN159_10570	2.3.1.-
pdeH	cyclic-guanylate-specific phosphodiesterase	71233..72000	GN159_09250	-
-	carboxylesterase family protein	53879..55387	GN159_00275	-
pdeR	cyclic di-GMP phosphodiesterase	158035..160026	GN159_00745	3.1.4.52

3.11. Modeling and validation of pesticide-degrading protein models in *Citrobacter* sp. HSTU-ABk15

3.11.1. Characterization of Pesticide-Degrading Protein Models in Citrobacter sp. HSTU-ABk15

Total twenty-five model proteins related to pesticide-degradation in *Citrobacter* sp. HSTU-ABk15 were identified and characterized (**Table 5**). The model proteins are belonged to several enzymes including amidohydrolases, Glp, Pep, Phn alongside AmpD, carboxylesterase, PdeH, and PdeR. The model proteins based on their best hit with PDB disclosed varied secondary structural composition with α-helix, β–strand, η-coil, and disordered regions. In consequence, a substantial number of models proteins established high quality as ERRAT scores was found directly above 85% for AmpD, GlpA, PepA, PepB, PepE, PhnF, PhnG, PhnH, PhnK, PhnL, and PhnO proteins. Likewise, VERIFY (3D-ID) score were remarkably high for PepA (99.80%), PepE (99.13%), GlpQ (97.49%), and PhnP (98.02%) proteins. In addition, PepA, PdeH, PepB, PepD, and PepE had placed residues 84.2%, 80.9%, 82.3%, 80.1%, 81.5% in the core region of Ramachandran plot. To strengthen the interpretation of the docking analysis, the quality and reliability of all modeled proteins were systematically evaluated using multiple complementary structural validation parameters prior to docking. These parameters directly indicate whether the predicted protein structures are suitable for ligand–protein interaction studies and whether the observed docking outcomes can be interpreted with confidence. The TM-score, RMSD, sequence identity, and coverage collectively demonstrate the structural reliability of the modeled proteins. Most proteins showed high TM-scores (>0.85) with low RMSD values (<2.0 Å)**,** indicating strong structural similarity to experimentally solved PDB templates. For example, AmpD, PepA, PepD, PepE, and PhnJ exhibited TM-scores ≥0.95 with RMSD values below 0.5 Å, reflecting highly accurate backbone conformations. Such structural fidelity ensures that predicted active-site geometry is preserved during docking simulations, thereby enhancing confidence in ligand binding poses and interaction energies. In contrast, proteins such as PhnD showed a markedly low TM-score (0.37) and high RMSD (8.04 Å), suggesting reduced structural confidence; docking results for these proteins were therefore interpreted cautiously. The proportion of α-helices, β-strands, coils, and disordered regions provides insight into structural stability and flexibility, both of which influence ligand binding. Most enzymes displayed balanced secondary structure distributions with low disordered regions (≤5%)**,** supporting the formation of well-defined binding pockets. Proteins with higher coil or disordered content (e.g., PhnD and PdeH) may exhibit greater conformational flexibility, potentially affecting docking precision and binding energy variability. ERRAT quality scores for most proteins exceeded 85%**,** and VERIFY-3D scores were generally above 80%**,** confirming favorable non-bonded atomic interactions and proper residue–environment compatibility. High ERRAT (e.g., PdeH: 97.97; PhnO:

99.25) and VERIFY-3D scores (e.g., PepA: 99.80; PepE: 99.13) indicate structurally sound models, supporting the biological relevance of docking-derived interactions. Lower scores (e.g., GlpB and PhnD) suggest potential local structural inaccuracies, which were considered when evaluating docking affinity rankings. Ramachandran statistics further validated stereochemical correctness. Most models exhibited >75–85% residues in the most favored (core) regions with minimal residues in disallowed regions (<2%), indicating proper backbone geometry. Proteins such as PepA, PhnG, and Amidohydrolase showed excellent conformational stability, strengthening the reliability of predicted ligand interactions within their active sites. Taken together, these parameters demonstrate that the majority of proteins used for docking possess high structural accuracy, correct stereochemistry, and stable secondary structures**,** which are prerequisites for meaningful docking analysis. Consequently, docking interactions observed for high-quality models (e.g., AmpD, Pep family proteins, PhnJ–PhnP) reliably reflect biologically plausible binding modes. Conversely, docking results for proteins with comparatively lower validation scores were interpreted qualitatively rather than quantitatively.

Table 5. Protein modeling and validation of pesticides degrading model proteins.

Model protein	Best PDB Hit	TM score, RMSD,Iden,cov	-helix, -strand - coll,disordered	ERRAT (quality score)	VERIFY (3D-ID score) %	Ramchandran plot (core, allow, gener, disallow) %
AmpD	1l2s	0.99,0.48,0.83,1.0	22,14,63,4	90.44	90.37	64.2,28.9,3.8,3.1
carboxylesterase	5x61	0.95,1.26,0.29,0.97	32,13,53,2	85.56	91.24	72.6,21.4,4.3,1.7
GlpA	2rgo	0.88,2.17,0.22,0.93	36,19,43,3	91.01	78.04	70.3,22.1,5.1,2.5
GlpB	1lpf	0.76,1.56,0.15,0.79	27,19,53,1	41.84	69.45	70.3,22.1,3.6,3.9
GlpQ	1ydy	0.91,0.37,0.89,0.91	29,14,56,8	85.42	97.49	74.9,18.5,5.3,1.3
PdeH	5m3c	0.93,1.50,0.23,0.98	40,19,40,7	97.97	63.53	80.9,14.8,2.2,2.2
PdeR	5xgb	0.81,0.68,0.26,0.81	42,22,34,1	54.04	76.47	80.8,12.8,3.6,2.8
PepA	1gyt	0.99,0.26,0.97,1.0	33,20,45,1	92.88	99.80	84.2,14.0,1.2,0.7
PepB	6cxd	0.96,0.34,0.76,0.97	33,19,47,0	95.46	94.38	82.3,15.3,1.3,1.1
PepD	3mru	0.99,0.28,0.63,1.0	28,25,46,2	92.24	97.32	80.1,16.7,1.7,1.4
PepE	1fye	0.95,0.29,0.85,0.96	26,26,47,1	95.00	99.13	81.5,14.3,4.2,0.0
PhnD	3vkg	0.37,8.04,0.05,0.63	47,17,35,8	66.15	59.32	50.0,33.9,11.3,4.8
PhnF	2wvo	0.98,0.52,0.19,0.98	29,32,38,4	94.37	86.72	76.6,19.3,2.8,1.4
PhnG	4xb6	0.92,1.21,0.68,0.96	45,25,29,5	97.10	72.67	87.4,9.6,1.5,1.5
PhnH	2fsu	0.85,0.71,0.83,0.86	26,21,52,6	96.23	87.63	73.8,22.6,1.8,1.8
PhnI	4xb6	0.97,1.19,0.87,0.99	38,12,48,5	89.34	46.20	81.6,15.2,1.6,1.6
PhnJ	4xb6	0.98,0.24,0.95,0.98	23,19,57,3	90.10	83.69	79.3,14.9,4.1,1.7
PhnK	4fwi	0.97,0.84,0.31,0.98	37,23,39,3	91.39	91.27	82.4,14.4,1.9,1.4
PhnL	5nik	0.92,1.18,0.27,0.96	33,26,39,1	92.27	96.63	73.8,19.8,4.5,2.0
PhnM	2oof	0.92,1.67,0.15,0.96	33,21,45,0	81.02	64.81	66.1,25.3,5.4,3.3
PhnO	5f46	0.91,1.42,0.18,0.99	34,31,34,2	99.25	86.11	73.6,17.1,5.4,3.9
PhnP	3g1p	0.98,0.38,0.80,0.99	11,28,59,0	87.96	98.02	72.5,22.2,3.4,1.9
Amidohyrolase (9962…10732)	2E11	0.96,0.34,0.76,0.97	22,33,43,1	76.61	84.38	87.1,12.1,0.4,0.4
Amidohyrolase Family protein (232305…234173)	3IGH	0.95,1.26,0.29,0.97	30,16,52,1	68.71	82.85	86.7,10.8,1.4,1.1
Amidohyrolase (6225..7358)	20GJ	0.76,1.56,0.15,0.79	27,23,49,2	69.12	85.03	83.7,13.2,1.2,1.8

3.11.2. Virtual screening and box plot of model protein and pesticide complex

The virtual screening of the selected 17 model proteins of HSTU-ABK15 with 99 different pesticides, shown binding score ranges from -9 Kcal/mol to -3 Kcal/mol (**Figure 5**). It is shown that most of the binding scores are occupied between the 1st and 3rd quartile in the box plot (**Figure 5)**, where the lower and upper quartile designates the 1st and 3rd quartile scores. Interestingly, total three model proteins (GlpA, PhnK, amidohydrolase II) of *Citrobacter* sp. HSTU-ABk15, were placed outlier data points. The virtual screening results also showed that the binding affinity of many pesticide ligands crossed over to -6.5~8.0 Kcal/mol for organophosphate degrading potential proteins AmpD, GlpQ, PepA, PepB, PepD, PepE, PhnF, PhnK, PhnL, PhnO, PhnP, and the amidohydrolase models proteins from *Citrobacter* sp. HSTU-ABK15**.**

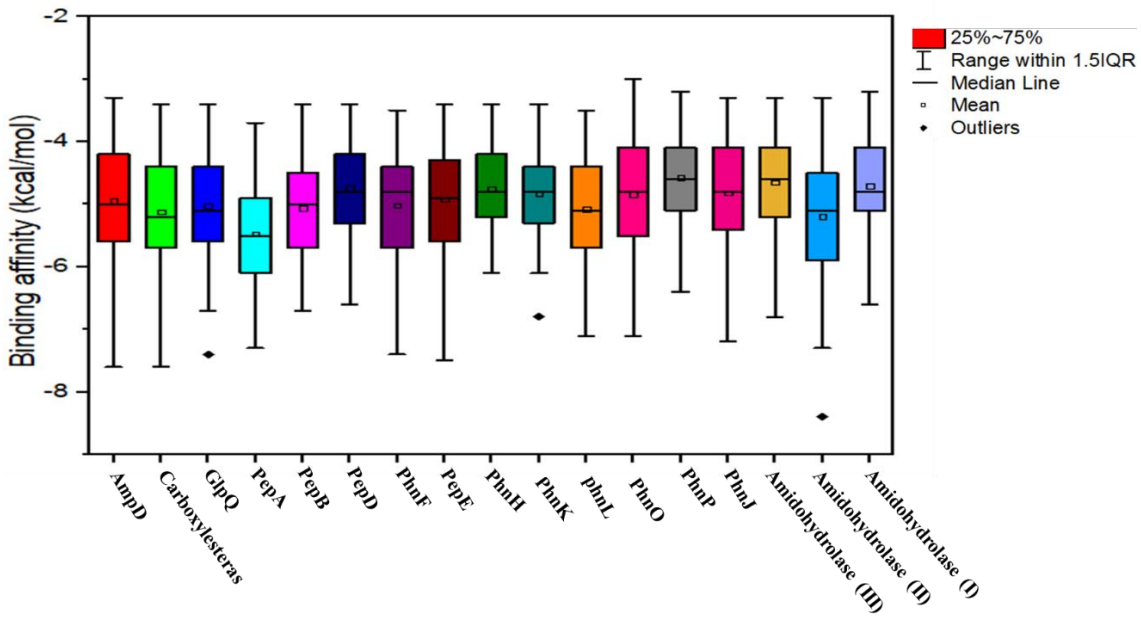

Figure 5. Graphical representation of virtual screening results of pesticide-degrading validated top scorer model proteins among 105 different organophosphorus pesticides and other common pesticides applied in farmers' fields.

3.11. 3. Docking and interactions of selected proteins of Citrobacter sp. HSTU-ABK15

Moreover, carboxylesterase protein-cypermethrin docked complex demonstrated the interaction with multiple residues. In particular, conventional H-bonds were made by the Ser195, His400 to the O-atom of cypermethrin compound. Besides, a great number of residues were interacted with the ligand molecule by alkyl, pi-alkyl, and pi-pi T-shaped bonds namely, Phe315, Val311, Pro121 and His108 sequentially (**Figure 6A)**. As seen in **Figure 6B**, the PepD is greatly interacted with diazinon through multiple amino acid residues. In fact, the O-atom in phosphodiester bond of diazinon is attacked by Ser170 via conventional H-bond. The Leu432, His76, His457Glu171, Tyr177 and Ile428 was provided alkyl, π-alkyl, π-anion, π-sulfur and carbon hydrogen bonds interaction with diazinon compound respectively. The Glu145 is providing conventional H-bond with N-H-atom of diazinon compound and Asp115 attached with the ligand by attractive charge. Astonishingly, the PepD of *Citrobacter* sp. HSTU-ABk15 formed potential catalytic triad in the binding pocket region with residue Ser170-

His457-Asp115. The interaction distances among the residues of catalytic site were recorded within <5.25 Å. These multiple interactions account for the good binding affinity of diazinon with pepD. Furthermore, PepE anchored with crotoxyphos compound revealed a great interaction (**Figure 6C**). Such as, Ser120 and Gly88 interacted with O atom of crotoxyphos molecule by conventional hydrogen bond. Besides, pi-alkyl, pi-pi-T shaped and carbon hydrogen bonds were made by Asp135, His157, Trp16, Tyr49 with crotoxyphos compound respectively.

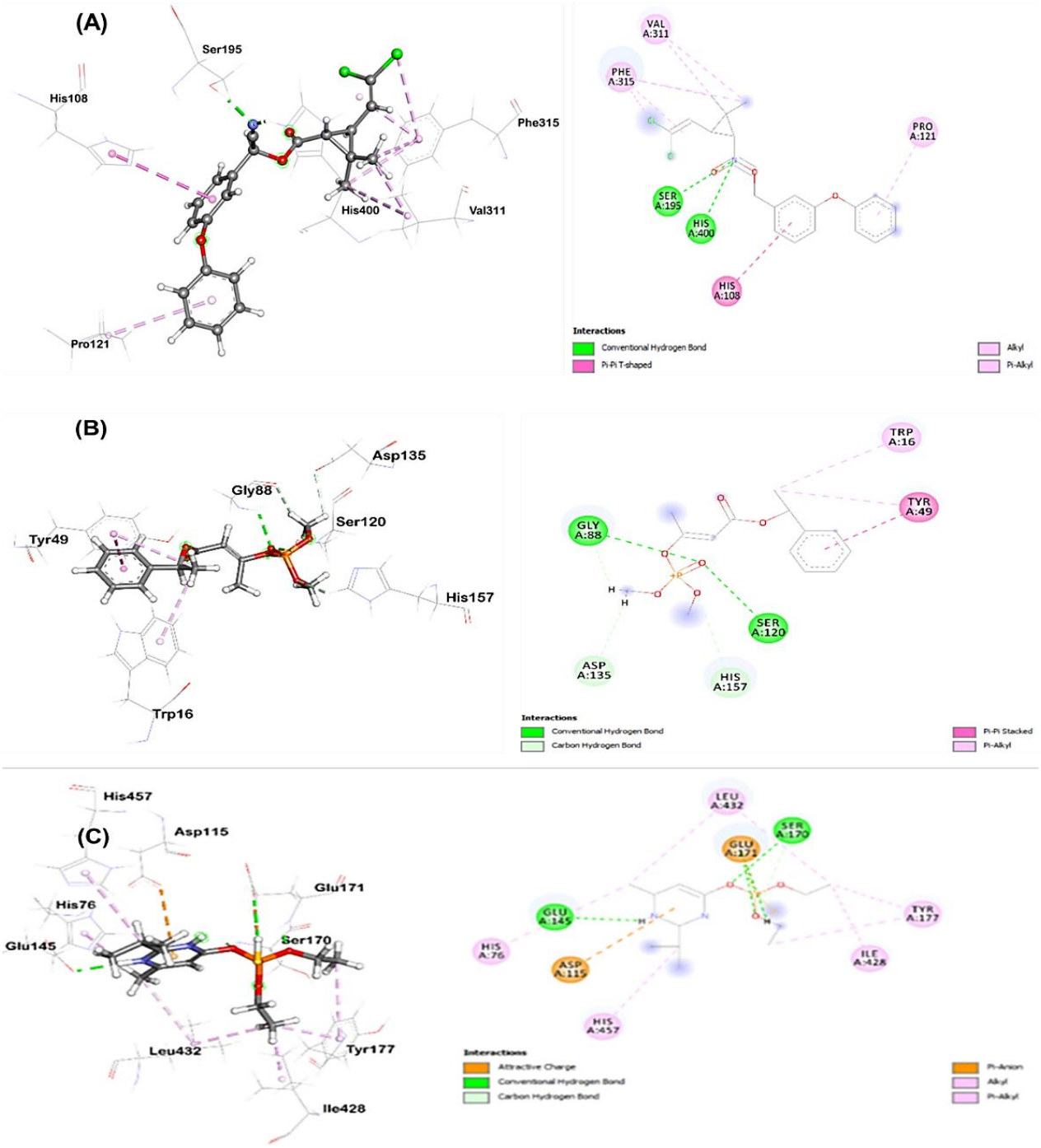

Figure 6. Catalytic triad's visualization of the complexes, A) carboxylesterase protein-cypermethrin**, B)** PepD protein-Diazinon, C) PepEprotein-Crotoxyphos.

4. DISCUSSION

The isolation of the multifunctional endophytic bacteria Citrobacter sp. HSTU-ABk15 from rice plants reveals a multiuse microbial consortium with broad ecological and biotechnological potential. These strains simultaneously harbored plant growth promotion, degrade the organophosphate pesticide chlorpyrifos, and exhibit antimicrobial biosynthetic potential, underscoring their capacity to address agricultural and environmental challenges through a unified biological framework [7, 21-23]. Distinct enzymatic profiles revealed adaptive metabolic versatility essential for endophytic colonization. Hydrolytic enzymes such as xylanase, amylase, protease, and CMCase suggest efficient host tissue penetration and nutrient [24-27]. Whole-genome sequencing confirmed close relationships to C. amalonaticus, supported by high ANI and dDDH values [28-29]. Functional annotation identified genes linked to nitrogen fixation, phosphate solubilization, ACC deaminase activity, and organophosphate degradation, reflecting a genomic architecture optimized for mutualistic and degradative functions [7,23,30]. These synergistic mechanisms affirm their potential as biofertilizers that could reduce chemical inputs while maintaining crop productivity under environmental constraints [21, 23, 31]. A pivotal finding of this study is the remarkable capacity of these endophytes for pesticides degradation insilico confirmation, offering a crucial eco-friendly solution for mitigating pesticide contamination and a significant step towards sustainable environmental management [7,18,32]. This multifaceted functionality highlights their promise for broader applications in bioremediation and sustainable agriculture [23]. Whole-genome sequencing confirmed close relationships to *C. amalonaticus*, supported by high ANI and dDDH values [28-29]. Although average nucleotide identity (ANI) and digital DNA-DNA hybridization (dDDH) values confirmed that the isolate belongs to *Citrobacter amalonaticus,* comparative genomic analysis revealed strain-specific genetic features associated with endophytic colonization, xenobiotic degradation, and plant growth–promoting functions. Therefore, the novelty of the isolate is defined at the strain level rather than at the species level. Functional annotation identified genes linked to nitrogen fixation, phosphate solubilization, ACC deaminase activity, and organophosphate degradation, reflecting a genomic architecture optimized for mutualistic and degradative functions [23, 30]. These synergistic mechanisms affirm their potential as biofertilizers that could reduce chemical inputs while maintaining crop productivity under environmental constraints [21, 23, 31]. A pivotal finding of this study is the remarkable capacity of these endophytes for pesticides degradation *insilico* confirmation, offering a crucial eco-friendly solution for mitigating pesticide contamination and a significant step towards sustainable environmental management [18, 32-33]. This multifaceted functionality highlights their promise for broader applications in bioremediation and sustainable agriculture [23].

Further molecular investigation unequivocally revealed the intricate enzymatic machinery facilitating this bioremediation, providing critical insights into its efficiency and specificity. Comprehensive characterization and quality validation of numerous pesticide-degrading model proteins from all three strains further corroborated their functional integrity, revealing high structural integrity, as evidenced by favorable ERRAT and VERIFY-3D scores, and optimal residue placement in Ramachandran plots. Reliable docking analysis depends critically on the structural accuracy and stereochemical quality of protein models [34]. Homology models were generated using templates from PDB and NCBI BLAST, with quality assessed via ProSA-web z-score and Ramachandran plot analysis using PROCHECK [34]. Secondary structure analysis revealed

proportions of α-helices, β-strands, turns, and coils [35-36]. Model quality assessment confirmed robustness, with VERIFY3D scores indicating compatibility of 3D atomic models with 1D amino acid sequences when >80% of residues score ≥0.2, and ERRAT scores evaluating non-bonded interactions where values >85-95% reflect high quality [37-40]. Ramachandran plot analysis evaluated stereochemical validity, with residues in core regions indicating good quality [34, 40]. Phn family members, such as those encoded by phnE and phnM, are involved in phosphonate transport and utilization [29]. Docking results for proteins in pesticide degradation pathways were interpreted with caution for models showing structural limitations [41]. Overall, integrated validation parameters using these tools confirm model quality suitable for docking in organophosphate degradation contexts [34,40,42]. Specifically, the models exhibited high percentages of residues in favored Ramachandran regions, typically exceeding 90%, and minimal outliers, ensuring reliable binding site geometries for ligand interactions [43].

Crucially, virtual screening against 99 different pesticides unearthed high binding affinities for numerous proteins with various organophosphate ligands, decisively pointing towards a remarkable broad-spectrum degradation potential. Molecular docking studies precisely elucidated the specific binding interactions at an atomic level: Ser195 and His400 in *Citrobacter* sp. HSTU-ABk15's carboxylesterase formed conventional H-bonds with cypermethrin; a potential catalytic triad in PepD interacted with diazinon via conventional H-bonds and other residues (**Figure 6**). These detailed molecular-level insights profoundly validate the observed degradation efficiencies and establish a comprehensive mechanistic framework for understanding the sophisticated endophyte-mediated xenobiotic detoxification processes. The established broad-spectrum degradation potential of these endophytes also suggests their applicability beyond chlorpyrifos to other organophosphorus pesticides, such as those found to be bioremediated by other bacterial species and earthworm associations [23]. The docking results suggest a strong potential for interaction between chlorpyrifos and several predicted enzymes, supporting their putative role in pesticide transformation. Although molecular docking and virtual screening provide valuable insights into enzyme–pesticide interactions, these approaches remain predictive in nature.

5. CONCLUSION

In conclusion, the endophytic bacterial strains, *Citrobacter* sp. HSTU-ABk15, isolated from rice, represent a powerful beneficial microorganism. Their demonstrated genetic repertoire in annotated genome having potentialities in effectively promoting rice plants growth, mediating comprehensive chlorpyrifos bioremediation through well-characterized enzymatic pathways, and exhibiting broad-spectrum antipathogenic activities, position them as highly promising candidates for sustainable biotechnological applications. The study primarily focuses on characterizing the endophytes and their potential beneficial traits, but it does not explicitly detail the molecular mechanisms within the rice plant itself that are influenced by these interactions. Future studies involving targeted enzymatic assays and analytical quantification of chlorpyrifos degradation products will be essential to experimentally validate the predicted degradation mechanisms. Subsequent research should prioritize the isolation, structural elucidation, and functional characterization of the resulting metabolites and associated enzymes to clarify their precise mechanisms of action and ecological interactions, thereby fully harnessing their potential for advancing sustainable agriculture and pharmaceutical innovation which is not substitute for molecular

dynamics simulations or experimental validation, which will be addressed in further studies for sustainable green agriculture.

ACKNOWLEDGEMENT

This work was supported by a research project grants by the Institute of research and Training (IRT)-Hajee Mohammad Danesh Science and Technology University, Dinajpur 5200. This study addresses about 10% AI-assisted text following the journal policy.

FUNDING SOURCES

This research was supported by the grants from the Institute of Research and Training (IRT)-Hajee Mohammad Danesh Science and Technology University (HSTU) in fiscal year 2021-2022 at Dinajpur, Bangladesh.

CONFLICTS OF INTEREST

The authors declare no conflicts of interest.

ETHICS STATEMENT

This study did not involve any experiments on human participants or animals; therefore, formal written informed consent was not required by the Institutional Review Board. All figures in this study were created; therefore, no permission for reuse is required for any figure presented herein.

DATA AVAILABILITY STATEMENT

The assembled and annotated genome sequence was deposited in the NCBI and provided accession number *Citrobacter* sp. HSTU-ABk15 (rice plant shoot) (Accession number: WQMR00000000; BioSample: SAMN13439369; BioProject: PRJNA592761)

REFERENCES

1. Basso MF, Neves MF, Grossi-de-Sá MF. Agriculture evolution, sustainability and trends focusing on Brazilian agribusiness: a review. *Front Sustain Food Syst.* 2024; 7:1296337. doi:10.3389/fsufs.2023.1296337
2. McKenzie FC, Williams J. Sustainable food production: constraints, challenges and choices by 2050. *Food Secur.* 2015;7(2):221-233.
3. Elhamalawy OH, Bakr A, Eissa F. Impact of pesticides on non-target invertebrates in agricultural ecosystems. *Pestic Biochem Physiol.* 2024; 202:105974. doi: 10.1016/j.pestbp.2024.105974
4. De P, Mondal N, Das SR, Uddin MJ, Ahmed MS, Al Billah M, et al. Prevalence of antibiotic-resistant bacterial contamination in local retail meat shops and hygiene practices by vendors. *J Biosci Public Health.* 2025;1(2):41-58. doi:10.5455/JBPH.2025.09
5. Kaur G, Patel AK, Dwibedi V, Rath SK. Harnessing the action mechanisms of microbial endophytes for enhancing plant performance and stress tolerance. *Arch Microbiol.* 2023;205(9):364. doi:10.1007/s00203-023-03643-4

6. Anand U, Pal T, Yadav N, Singh VK, Tripathi V, Choudhary KK, et al. Current scenario and future prospects of endophytic microbes for agricultural and environmental sustainability. *Microb Ecol.* 2023;86(3):1455-1474. doi:10.1007/s00248-023-02190-1
7. Haque MA, Hossain MS, Ahmad I, Akbor MA, Rahman A, Manir MS, et al. Chlorpyrifos mineralization and plant growth promotion by *Enterobacter* sp. strain HSTU-ASh6. *Front Microbiol.* 2022; 13:1060554. doi:10.3389/fmicb.2022.1060554
8. Kumar P, Arshad M, Gacem A, Soni S, Singh S, Kumar M, et al. Environmental fate and sustainable degradation of chlorpyrifos. *Environ Sci Pollut Res Int.* 2023;30(50):108347-108365. doi:10.1007/s11356-023-30049-y
9. Zakariyah RF, Ajijolakewu KA, Ayodele AJ, Folami-A BI, Samuel EP, Otuoze SO, et al. Endophytic fungi secondary metabolites: biosynthetic gene cluster reactivation. *Bull Natl Res Cent.* 2024; 48:44. doi:10.1186/s42269-024-01199-x
10. Malfent F, Zehl M, Kirkegaard RH, Oberhofer M, Zotchev SB. Genomes and secondary metabolomes of *Streptomyces* spp. *Front Microbiol.* 2024; 15:1408479. doi:10.3389/fmicb.2024.1408479
11. Haque MA, Lee JH, Cho KM. Endophytic bacterial diversity in kimchi and antimicrobial activity. *Food Control.* 2015; 56:24-33. doi: 10.1016/j.foodcont.2015.03.006
12. Das SR, Haque MA, Akbor MA, Abdullah-Al-Mamun M, Debnath GC, Hossain MS, et al. Organophosphorus insecticide-mineralizing bacterial consortium promotes eggplant growth. *Arch Microbiol.* 2022;204(3):199. doi:10.1007/s00203-022-02809-w
13. Abdullah-Al-Mamun M, Hossain MS, Debnath GC, Sultana S, Rahman A, Hasan Z, et al. Lignocellulolytic traits of *Klebsiella variicola* strain HSTU-AAM51. *Braz J Microbiol.* 2022;53(1):99-130. doi:10.1007/s42770-021-00660-7
14. Sharker B, Islam MA, Hossain MAA, Ahmad I, Al Mamun A, Ghosh S, et al. Lignin- and hemicellulose-degrading bacteria for rice straw deconstruction. *Sci Total Environ.* 2023; 904:166704. doi: 10.1016/j.scitotenv.2023.166704
15. Haque MA, Simo S, Prodhan MY, Ghosh S, Hossain MS, Rahman A, et al. Diazinon-mineralizing endophytic bacteria enhance rice growth. *Arch Microbiol.* 2023;205(6):231. doi:10.1007/s00203-023-03564-2
16. Singh BK, Walker A. Microbial degradation of organophosphorus compounds. *FEMS Microbiol Rev.* 2006;30(3):428-471.
17. Mashrur MN, Hasan MR, Sultana S, Boby M, Das M, Abrar S, et al. Structural and functional analysis of a hypothetical protein in *Saccharomyces cerevisiae*. *J Biosci Public Health.* 2025;1(3):79-97. doi:10.5455/JBPH.2025.16
18. Lee HY, Cho DY, Ahmad I, Patel HM, Kim MJ, Jung JG, et al. Mining of a novel esterase gene degrading organophosphorus insecticide. *Int J Biol Macromol.* 2021; 190:441-455. doi: 10.1016/j.ijbiomac.2021.08.224
19. Haque AM, Hwang CE, Kim SC, Cho DY, Lee HY, Cho KM, et al. Biodegradation of organophosphorus insecticides by *Leuconostoc mesenteroides*. *Process Biochem.* 2020; 94:340-348. doi: 10.1016/j.procbio.2020.04.026
20. Zhang Y. I-TASSER: fully automated protein structure prediction in CASP8. *Proteins.* 2009;77(Suppl 9):100-113. doi:10.1002/prot.22588
21. Feng F, Ge J, Li Y, He S, Zhong J, Liu X, et al. Endophytic bacteria enhance chlorpyrifos degradation in rice. *Chemosphere.* 2017; 184:505-513. doi: 10.1016/j.chemosphere.2017.05.178
22. Nawaz A, Mubeen F, Qamar ZU, Marghoob MU, Aziz S, Gross H. Draft genome sequence of *Citrobacter braakii* AN-PRR1. *Microbiol Resour Announc.* 2021;10(38): e00787-21. doi:10.1128/mra.00787-21
23. Prodhan MY, Rahman MB, Rahman A, Akbor MA, Ghosh S, Nahar MNEN, et al. Chlorpyrifos-mineralizing endophytic bacterial consortia as biostimulants. *Microorganisms.* 2023;11(7):1821. doi:10.3390/microorganisms11071821
24. Awasthi S, Wadhwa N. Screening of plant growth-promoting endophytes of wheat. *Curr Appl Sci Technol.* 2023;23(6):006. doi:10.55003/cast.2023.06.23.006
25. Doğan G, Taşkın B. Hydrolytic enzyme-producing bacterial endophytes of Poaceae plants. *Pol J Microbiol.* 2021;70(3):297-306. doi:10.33073/pjm-2021-026
26. Petrović M, Janakiev T, Grbić ML, Unković N, Stević T, Vukićević S, et al. Endophytic and rhizospheric bacteria of sugar beet hybrids. *Microb Ecol.* 2023;87(1):114-130. doi:10.1007/s00248-023-02329-0
27. Walitang DI, Kim K, Madhaiyan M, Kim YK, Kang Y, Sa T. Endophytic competence and plant growth promotion in rice seed endosphere. *BMC Microbiol.* 2017; 17:209. doi:10.1186/s12866-017-1117-0
28. Faccone D, Albornoz E, Tijet N, Biondi E, Gómez S, Pasterán F, et al. Multidrug-resistant *Citrobacter amalonaticus* harboring blaNDM-1 and mcr-1.5. *Infect Genet Evol.* 2018; 67:51-55. doi: 10.1016/j.meegid.2018.10.020
29. Rey-Velasco X, Lucena T, Belda A, Gasol JM, Sánchez O, Arahal DR, et al. Genomic and phenotypic characterization of novel marine bacteria. *Front Microbiol.* 2024; 15:1407904. doi:10.3389/fmicb.2024.1407904
30. Ganie SA, Bhat JA, Devoto A. Influence of endophytes on rice fitness under environmental stress. *Plant Mol Biol.* 2021; 109:447-459. doi:10.1007/s11103-021-01219-8
31. Shan S, Cheng WS, Li Y, Zhang M, Liu Z, Wang Y, et al. Comparative genomics of *Citrobacter* sp. XT1-2-2. *BMC Genomics.* 2022; 23:792. doi:10.1186/s12864-022-09069-4
32. Bhagawati S, Bhattacharyya B, Bhattacharjee S, Devi EB, Manpoong NS, Das PP. Microbial bioremediation of pesticide residues. *Int J Curr Microbiol Appl Sci.* 2020;9(4):1551-1563. doi:10.20546/ijcmas.2020.904.182
33. Raffa CM, Chiampo F. Bioremediation of agricultural soils polluted with pesticides. *Bioengineering.* 2021;8(7):92. doi:10.3390/bioengineering8070092
34. Gupta S, Mandal A, Ghosh A, Kundu A, Saha S, Singh A, et al. Insecticidal potential of alkaloids against *Thrips palmi*. *Sci Rep.* 2024; 14:77236. doi:10.1038/s41598-024-77236-6

35. Hasan MA, Mazumder MHH, Chowdhury A, Datta A, Khan MA. Molecular docking of transketolase in *Plasmodium falciparum*. *Source Code Biol Med.* 2015; 10:7. doi:10.1186/s13029-015-0037-3
36. Maia TR, Filho MMR, Campos M, eds. *Homology Molecular Modeling: Perspectives and Applications.* IntechOpen; 2021. doi:10.5772/intechopen.91624
37. Chakma V, Barman DN, Das SC, Hossain A, Momin MB, Tasneem M, et al. In silico analysis of a hypothetical protein from *Staphylococcus aureus*. *J Genet Eng Biotechnol.* 2023;21(1):135. doi:10.1186/s43141-023-00613-7
38. Hamid M, Habib U, Batool J, Qaisar A, Paracha RZ. Computational structural analysis of MOCS1. *Res Sq.* 2021. doi:10.21203/rs.3.rs-473901/v1
39. Mohtar JA, Shahimin MFM, Bakar ARA, Rahman KHA. In silico modeling of ampullate spidroin N-terminal domain. *Res Sq.* 2024. doi:10.21203/rs.3.rs-3968553/v1
40. Sankar S, Ramamurthy M, Nandagopal B, Sridharan G. In silico validation of *Aedes aegypti* D7 salivary protein epitopes. *Bioinformation.* 2017;13(11):366-372. doi:10.6026/97320630013366
41. Spyrakis F, Cavasotto CN. Challenges in structure-based virtual screening. *Arch Biochem Biophys.* 2015; 583:105-119. doi: 10.1016/j.abb.2015.08.002
42. Latip W, Knight VF, Halim NA, Ong KK, Kasim NAM, Yunus WMZW, et al. Microbial phosphotriesterase: structure and applications. *Catalysts.* 2019;9(8):671. doi:10.3390/catal9080671
43. Corrêa EJA, Carvalho FC, Oliveira JAC, Bertolucci SKV, Scotti MT, Silveira CH, et al. Molecular mechanisms of essential oils' insecticidal action. *Sci Rep.* 2023; 13:29981. doi:10.1038/s41598-023-29981-3